May 24, 2008
Revised June 24, 2008

arXiv:0806.0890v2 [hep-ph] 25 Jun 2008

# A $Z'$ Boson and the Higgs Boson Mass

Michael S. Chanowitz

*Theoretical Physics Group*
*Lawrence Berkeley National Laboratory*
*University of California*
*Berkeley, California 94720*

**Abstract**

The Standard Model fit prefers values of the Higgs Boson mass $m_H$ that are below the 114 GeV direct lower limit from LEP II. The discrepancy is acute if the $3.2\sigma$ disagreement for $\sin^2\theta_W^{\ell\ \mathrm{eff}}$ from the two most precise measurements is attributed to underestimated systematic error. In that case the data suggests new physics to raise the predicted value of $m_H$. One of the simplest possibilities is a $Z'$ boson, which would generically increase the prediction for $m_H$ as a result of $Z$-$Z'$ mixing. We explore the effect of $Z$-$Z'$ mixing on the $m_H$ prediction, using both the full data set and the reduced data set that omits the hadronic asymmetry measurements of $\sin^2\theta_W^{\ell\ \mathrm{eff}}$, which are more likely than the leptonic asymmetry measurements to have underestimated systematic uncertainty.

## 1. Introduction

The Standard Model fit of the precision electroweak data, reviewed below, has a less than robust $\chi^2$ confidence level, $CL(\chi^2, N) = CL(17.2, 12) = 0.14$, as a result of the enduring $3.2\sigma$ discrepancy between the two most precise measurements of the effective leptonic weak mixing angle, $\sin^2\theta_W^{\ell\ \mathrm{eff}}$, from the polarization asymmetry $A_{LR}$ and the front-back $b$ quark asymmetry $A_{FB}^b$. Since the SM fit is relied on to provide guidance on the mass of the Higgs boson, it is relevant to consider the consistency of the sector of measurements that predict the value of $m_H$. In this sector the problem is more severe, with $CL(\chi^2, N) = CL(14.1, 7) = 0.05$. The discrepancy between $A_{LR}$ and $A_{FB}^b$ is reflected in a $3.2\sigma$ discrepancy between the three leptonic asymmetry measurements, $A_{LR}$, $A_{FB}^\ell$, $A_\ell(P_\tau)$, and the three hadronic asymmetry measurements, $A_{FB}^b$, $A_{FB}^c$, and $Q_{FB}$, and in the poor $\chi^2$ for the combination of all six asymmetries, $CL(11.8, 5) = 0.037$.[1] These discrepancies could be statistical fluctuations, evidence of new physics, or the result of underestimated systematic uncertainty. If they are due to new physics, we cannot extract the Higgs boson mass $m_H$ from the precision data without first specifying the nature of the new physics.

It might appear that the viability of the SM could be enhanced if the discrepancies are attributed to underestimated systematic uncertainty, in particular, in the hadronic asymmetry measurements, which share challenging, common experimental and theoretical systematic uncertainties. Indeed, if that is assumed and the three hadronic asymmetry measurements are omitted from the fit, the confidence level increases from 0.14 to 0.78, but a new problem emerges: the remaining measurements, dominated by $A_{LR}$ , $m_W$, and $m_t$, predict $m_H = 50$ GeV, with only a small probability, $CL(m_H > 114) = 0.03$, for $m_H$ in the region $m_H > 114$ GeV allowed by the LEP II direct search limit.[2] Therefore this scenario also suggests new physics, in this case new physics to raise the predicted value of $m_H$, and once again $m_H$ cannot be extracted from the data without specifying a model for the new physics.

With this motivation several models of new physics have been considered to raise the the predicted value of $m_H$ in the fit with hadronic asymmetries excluded, including light sneutrinos and gauginos,[3] a fourth family of quarks and leptons,[4] and mixing with heavy vector-like leptons[5]. In this paper we consider mixing of the SM $Z$ boson with a heavy $Z'$ boson associated with a new Abelian symmetry with generator $Q_X$, a simple extension of the SM that can raise the predicted value of $m_H$. The mechanism is easy to understand: a heavy Higgs boson makes a negative contribution to the $\rho$ parameter, $\rho = m_W^2/m_Z^2\cos^2\theta_W$, while mixing of $Z$ with a heavier $Z'$ shifts $m_Z$ downward, causing $\rho$ to increase so that the two effects tend to cancel. This possibility has been explored by Ferroglia, Lorca, and van der Bij[6] for the reduced data set with $A_{FB}^b$ excluded, for $Z'$ bosons coupled to weak hypercharge $Y$ and to $B - L$, the difference of baryon and lepton number. Our results agree qualitatively with theirs but differ in detail, both in the formulation of the $Z'$ model and in

the implementation of the experimental constraints. In our approach but not in theirs the $Z$-$Z'$ mass matrix is generated by Higgs bosons in the conventional way.[1] This theoretical difference has experimental consequences which are discussed below. They fit a truncated data set that captures the principal features but differs in detail from our fits, which are based on the complete EWWG[1] data set, use ZFITTER[7] to compute the radiative corrections, and include the largest experimental correlations as given by the EWWG. In addition, we impose the constraints on $Z'$ production extracted by Carena *et al.*[8] from the LEP II bounds for BSM contact interactions,[9] which we find are stronger than the precision EW constraints in parts of the $Q_X$ parameter space. We also impose the more recent constraints on $Z'$ models obtained by the CDF collaboration,[10] which are stronger than the LEP II bounds for some of the $Q_X$ parameter space if the $Z'$ coupling constant is sufficiently small,[2] in particular, smaller than electroweak strength. Fits both with and without the hadronic asymmetries are presented.

Following [11, 12] we consider a class of models in which (1) the $Z'$ receives its mass from a heavy SM singlet Higgs boson $H'$, (2) the new gauge group $U(1)_X$ is required to be anomaly free with matter fields restricted to three SM generations augmented only by three right-handed neutrinos, and (3) the $Q_X$ charges of the SM fermions are independent of generation. It then follows[11, 12] that $Q_X$ must act on quarks and leptons like a linear combination of SM hypercharge $Y$ and $B-L$, say[3]

$$Q_X = \cos\theta_X \frac{Y}{2} + \sin\theta_X \frac{B-L}{2}. \tag{1}$$

The SM fermions and the $W^\pm, Z_0$ bosons obtain their masses from the usual SM Higgs boson, which to preserve $Q_X$ gauge invariance must also be assigned $Q_X$ charge $\cos\theta_X \frac{Y}{2} + \sin\theta_X \frac{B-L}{2}$ with its usual SM $Y$ and (vanishing) $B-L$ charges. In this approach, in order for there to be $Z$-$Z'$ mass mixing, the SM Higgs boson must have nonvanishing $Q_X$ charge, $Q_X H \neq 0$, requiring $|\theta_X| \neq \pi/2$. This contrasts with the model of [6] in which $Z$-$Z'$ mixing can occur even if $Q_X$ acts on SM quanta purely like $B-L$. Following [12], we use the freedom to define the SM $B$-hypercharge gauge boson and the new singlet $Z'$ so that kinetic mixing vanishes at the electroweak scale and $Z$-$Z'$ mixing is completely described by the mass matrix for the relevant energies near the TeV scale. We assume the SM singlet Higgs boson $H'$ has a very large vacuum expectation value, $v' \gg v$, and that the new vector boson is much heavier than the $Z$, $m_{Z'} \gg m_Z$.

[1] The authors of [6] exploit the fact that the Higgs mechanism is not necessary to ensure renormalizability in the case of Abelian gauge bosons.

[2] I thank Bogdan Dobrescu for bringing the CDF bounds to my attention.

[3] A peculiar third solution obtained in [11] is incorrect, because those authors apparently failed to consider the $SU(3)_C^2 \times U(1)_X$ anomaly.

$Q_X$ then coincides with the SM generators $\cos\theta_X \frac{Y}{2} + \sin\theta_X \frac{B-L}{2}$ in its action on SM matter quanta but not in its action on BSM quanta such as $H'$. In this framework with $\theta_X = 0$ there can be a class of "$Y$-sequential" $Z'$ bosons with charges $Y'$ which are identical to the SM hypercharge $Y$ in their action on SM quanta but differ in their action on BSM quanta.[11, 12] These models were described as "unaesthetic" in [11], although with a caveat that did not survive the journal's editorial process but is reproduced here: "We are humbly aware that aesthetic judgements are subjective and time-dependent. The cockroaches of Troy probably did not understand why the Greeks were making so much fuss."[4] This class of models has an appreciable effect on the allowed range of $m_H$ in the EW fits, and especially for the fit of the reduced data set.

The issues raised by the precision EW data will continue to be important in the era of the LHC. Just as it has played an important role in the development of the SM, the precision EW data can also help us to understand the discoveries that will be made at the LHC. But our ability to use the precision EW data for this purpose will be severely limited if we cannot resolve the ambiguity created by the $A^b_{FB}$ anomaly.

In section 2 we review the SM fit and predictions for the Higgs boson mass. In section 3 we describe the class of $Z'$ models to be considered. In section 4 we summarize the relevant LEP II constraints on $Z'$ bosons, taken from [8] and [9], and the more recent constraints from CDF.[10] In section 5 we present constraints from the fits to the precision electroweak data together with the LEP II constraints. Concluding remarks are given in section 6. In an appendix we show that for a $Y$-sequential $Z'$ the effect of $Z - Z'$ mixing on the SM fit can be fully represented by "pseudo-oblique" corrections, which account for both vacuum polarization and vertex corrections.

## 2. The Standard Model Fit

In this section we review the SM fit to the precision electroweak data. We use the data set and methodology of the EWWG[1] with one exception: we do not include the $W$ boson width in our fits, since with a 2.5% error it is not a precision measurement in the sense of the others, which are typically measured to O(0.1%) or better, and in any case it has no impact on the prediction for the Higgs boson mass. We include the largest experimental correlations as given by the EWWG and use ZFITTER[7] to compute the radiative corrections, including the two loop contributions to $\sin^2\theta_W^{\ell\,\mathrm{eff}}$ amd $m_W$.[13] Like the EWWG we perform a $\chi^2$ fit to the data, scanning over $m_t, \Delta\alpha^{(5)}_{\mathrm{had}}(m_Z), \alpha_S(m_Z)$, and $m_H$,[5] leaving the latter two parameters unconstrained. The fits use the most recent Fermilab measurement of the top quark mass,[14]

[4] See the footnote on page 10 of the scanned preprint of [11] posted at http://ccdb4fs.kek.jp/cgi-bin/img_index?197706199.

[5] We have verified that the fit is not affected by scanning on $m_Z$ because it is much more precisely measured than the other observables.

| | Experiment | EWWG SM Fit | Our SM Fit | Pull |
|---|---|---|---|---|
| $A_{LR}$ | 0.1513 (21) | 0.1480 | 0.1480 | 1.6 |
| $A^l_{FB}$ | 0.01714 (95) | 0.01643 | 0.01642 | 0.76 |
| $A_{e,\tau}$ | 0.1465 (32) | 0.1480 | 0.1480 | -0.45 |
| $A^b_{FB}$ | 0.0992 (16) | 0.1038 | 0.1037 | -2.8 |
| $A^c_{FB}$ | 0.0707 (35) | 0.0742 | 0.0741 | -1.0 |
| $x^l_W[Q_{FB}]$ | 0.2324 (12) | 0.2314 | 0.2314 | 0.83 |
| $m_W$ | 80.398 (25) | 80.377 | 80.374 | 0.95 |
| $\Gamma_Z$ | 2495.2 (23) | 2495.9 | 2495.9 | -0.3 |
| $R_l$ | 20.767 (25) | 20.743 | 20.744 | 1.0 |
| $\sigma_h$ | 41.540 (37) | 41.478 | 41.477 | 1.7 |
| $R_b$ | 0.21629 (66) | 0.21581 | 0.21586 | 0.65 |
| $R_c$ | 0.1721 (30) | 0.1722 | 0.1722 | -0.04 |
| $A_b$ | 0.923 (20) | 0.935 | 0.935 | -0.6 |
| $A_c$ | 0.670 (27) | 0.668 | 0.668 | 0.07 |
| $m_t$ | 172.6 (1.4) | 172.8 | 172.3 | 0.24 |
| $\Delta\alpha_5(m_Z^2)$ | 0.02758 (35) | 0.02767 | 0.02768 | 0.29 |
| $\alpha_S(m_Z)$ | | 0.1185 | 0.1186 | |
| $m_H$ | | 87 | 85 | |

Table 1: SM fit compared with the EWWG fit.[15]

$m_t = 172.6 \pm 1.4$ GeV.

In table 1 our fit is compared with the most recent EWWG fit[15], where it is clear the two are virtually indistinguishable: with $\Gamma_W$ omitted both yield $\chi^2/N = 17.2/12$ (with correlations contributing $-1.4$). The difference for $m_t$ is an artifact of our fitting grid, $\Delta m_t = .21$ GeV, which has been overtaken by the increasing experimental precision. The consistency for all other quantities, one part per *mil* or better, shows that the coarseness of the $m_t$ grid has not affected the quality of the fit. For the Higgs mass our central value is 85 GeV, indistinguishable from 87 GeV obtained by the EWWG.

We can see from table 1 that the less than robust $\chi^2$ confidence level of the SM fit, $CL(17.2, 12) = 0.14$, is a consequence of the 3.2 $\sigma$ discrepancy between the leptonic and hadronic asymmetry measurements. $A^b_{FB}$ is the measurement with the largest pull, $2.82\sigma$, corresponding to a a nominal Gaussian confidence level of 0.0048. The significance of such an outlyer can be estimated by the probability that one of twelve independent measurements will fluctuate to $\geq 2.82\sigma$, which is $1 - (1 - 0.0048)^{12} = 0.06$, enough by itself to account for

| | $m_H$ (GeV) | 90% $CL$ | $CL(m_H > 114)$ |
|---|---|---|---|
| $A_{LR}$ | 34 | $10- < m_H < 108$ | 0.07 |
| $m_W$ | 52 | $15 < m_H < 135$ | 0.10 |
| $A^b_{FB}$ | 480 | $170 < m_H < 1000+$ | 0.99 |
| $A_{LR} \oplus A^l_{FB} \oplus A_\tau$ | 50 | $19 < m_H < 126$ | 0.07 |
| $m_W \oplus \Gamma_Z \oplus R_l$ | 52 | $10 < m_H < 140$ | 0.10 |
| $A^b_{FB} \oplus A^c_{FB} \oplus Q_{FB}$ | 480 | $180 < m_H < 1000+$ | 0.99 |

Table 2: Predictions for $m_H$ from various restricted sets of $m_H$-sensitive observables. The value of $m_H$ at the $\chi^2$ minimum is shown along with the symmetric 90% confidence interval and the likelihood for $m_H > 114$ GeV. 10− and 1000+ denote intervals extending below 10 or above 1000 GeV.

the less than robust confidence level of the global fit. If we consider only the observables that are sensitive to $m_H$, omitting $R_b, R_c, A_b, A_c, \sigma_H$ which are not, the $\chi^2$ confidence level falls by a factor 3 to $CL(14.1, 7) = 0.05$, and $A^b_{FB}$ is again the leading outlyer with a pull of $2.80\sigma$ and nominal likelihood 0.0051. The probability for such an outlyer is then $1-(1-0.0051)^7 = 0.035$, which matches nicely with the 0.05 confidence level of the corresponding $\chi^2$ fit. For both of these fits the central value for the Higgs boson mass is $m_H = 85$ GeV, but since $CL(m_H > 114) = 0.26$ there is no significant conflict with the LEP II 114 GeV lower limit.

It is instructive to consider why $A^b_{FB}$ is the outlyer in these fits rather than $A_{LR}$. The explanation is that there is an "alliance" between the leptonic asymmetry measurements and the $W$ boson mass against the hadronic asymmetry measurements. The former favor very low values for the Higgs boson mass, $m_H \lesssim 50$ GeV, as opposed to the hadronic asymmetry measurements, which predict $m_H$ an order of magnitude heavier, $m_H \simeq 500$ GeV. In table 2 the central value from a fit to $A^b_{FB}$ alone is $m_H = 480$ GeV, while $A_{LR}$ and $m_W$ predict values an order of magnitude smaller, $m_H = 34$ and 52 GeV respectively. We see in table 2 and figure 1 that these differences are significant: the 90% symmetric confidence intervals for $m_H$ from the leptonic asymmetries and from the nonasymmetry measurements do not overlap the 90% interval from the hadronic asymmetries. (Note that the 95% confidence level upper limit is just the upper limit of the symmetric 90% confidence interval.)

The interpretation of the precision data then depends critically on how we interpret the discrepancy between the hadronic and leptonic asymmetry data. If it is a statistical fluctuation then the prediction for $m_H$ from the $\chi^2$ fit to the full data set is applicable, with central value 85 GeV and 95% upper limit 158 GeV. Since the $A^b_{FB}$ and $A_{LR}$ measurements both represent many years of careful work, it is also certainly possible that the discrepancy

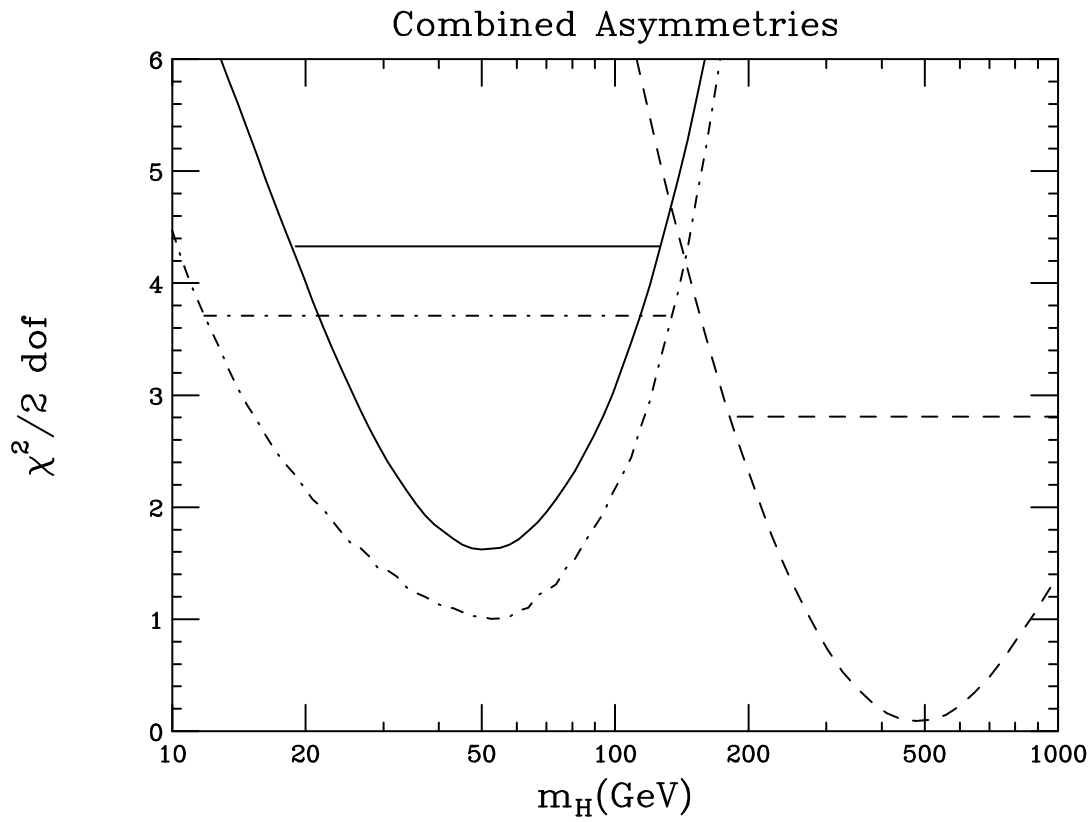


Figure 1: $\chi^2$ distributions as a function of $m_H$ from the combination of the three leptonic asymmetries $A_{LR}$, $A^{\ell}_{FB}$, $A_{\ell}(P_{\tau})$ (solid line); the three hadronic asymmetries $A^{b}_{FB}$, $A^{c}_{FB}$, and $Q_{FB}$ (dashed line); and the three $m_H$-sensitive, nonasymmetry measurements, $m_W, \Gamma_Z$, and $R_l$ (dot-dashed line). The horizontal lines indicate the respective 90% symmetric confidence intervals.

is a genuine reflection of new physics, for instance, in the $Z\bar{b}b$ vertex. Because $R_b$ agrees well with the SM prediction, it is straightforward to show that this hypothesis requires a very large ($\sim 20\%$) new physics contribution to the right-handed $Z\bar{b}b$ coupling. Popular models of new physics cannot readily explain the data, but there is not a no-go theorem and some possibilities have been explored.[16] If it is a genuine manifestation of new physics, then the new physics must first be known in order to use the precision data to predict $m_H$.

The third possible explanation of the discrepancy is underestimated systematic error. The three leptonic measurements are comparatively straightforward. They are free of complications from QCD and hadronization, involve three quite different techniques with no common systematic uncertainties, and have a sensible $\chi^2$, with $\sin^2\theta_W^{\ell\,\mathrm{eff}} = 0.23113$ (21) and $CL(1.6/2) = 0.44$. In contrast, the three hadronic measurements share challenging experimental and theoretical systematic issues, including heavy flavor tagging, large QCD corrections, and, especially, reliance on hadronic Monte Carlo simulations to merge the QCD

| | $m_H$ (GeV) | 90% $CL$ | $CL(m_H > 114)$ |
|---|---|---|---|
| All data | 85 | $47 < m_H < 158$ | 0.26 |
| $A^b_{FB} \oplus A^c_{FB} \oplus Q_{FB}$ excluded | 50 | $24 < m_H < 105$ | 0.03 |

Table 3: Predictions for $m_H$ from fits with and without the hadronic asymmetries.

corrections with the experimental acceptance. They combine to give $\sin^2\theta_W^{\ell\ \mathrm{eff}} = 0.23222\ (27)$ with $CL(0.02/2) = 0.99$. The surprisingly small $\chi^2$ results from an underlying 14 parameter heavy flavor fit, with an even more surprising $\chi^2$, $CL(53, 91) = 0.9995$. These small $\chi^2$ values could result from overestimated systematic errors, but then the significance of the discrepancy is exacerbated and the fit CL decreases: e.g., using just statistical errors for the three hadronic measurements the $\chi^2$ of the SM fit increases to 20.2/12 and the CL falls to 0.06. Another possible explanation of the small $\chi^2$ values is that they reflect incompletely understood correlations, which would again point to the possiblity of underestimated systematic error. A more detailed discussion is given in the talk cited in [2].

Only future experimental results can help us to choose among the three possible explanations. In this work we focus on the third possibility, not because we know it to be more likely but rather to understand the consequences. It might appear at first glance that the problem for the SM would be resolved if the three hadronic asymmetry measurements are assumed to have underestimated systematic errors and are omitted from the fit. The $\chi^2$ fit is then robust, with the p-value increasing from $CL(17.2, 12) = 0.14$ to $CL(5.63, 9) = 0.78$, but the prediction for $m_H$ becomes problematic, with central value $m_H = 50$ GeV, with the 95% CL upper limit at $m_H = 105$ GeV, and with only 3% probability in the region allowed by the LEP II lower bound, $CL(m_H > 114) = 0.031$, excluding the SM at $\simeq 97\% CL$. The $m_H$ predictions from the two fits are summarized in table 3.

One might think since the $\chi^2$ CL and $CL(m_H > 114)$ are independent probabilities that their product would be a measure of the likihood that the data agrees with the SM both as to the precision measurements and the Higgs mass prediction. However the product is not a fair estimator because it does not reflect the many ways that two independent probabilities can yield a product of a given value $P_1P_2$. A better estimator is the combined probability $P_C$ that the product of two independent, uniformly distributed probabilities is less than or equal to the product $P_1P_2$, which it is easy to show is given by

$$P_C(P_1P_2) = P_1P_2(1 - \log(P_1P_2)). \tag{2}$$

The fit to all data then yields $P_C(0.14 \cdot 0.26) = 0.16$, little changed from the $\chi^2$ likelihood alone, while the reduced fit yields a somewhat smaller value, $P_C(0.78 \cdot 0.03) = 0.11$. Clearly

the consistency of the SM with the data is not improved by removing the hadronic asymmetry measurements but rather the nature of the problem changes while remaining no less severe.

Like the discrepancy between the hadronic and leptonic asymmetry measurements, the conflict of the reduced data set with the LEP II bound also has the canonical three possible generic explanations: new physics, systematic error or statistical fluctuation. We focus here on the possibility that it is an indicator for new physics, and consider below a class of $Z'$ models that can maintain the quality of the $\chi^2$ fit for the reduced data set while raising the $m_H$ prediction into the allowed region above 114 GeV.

## 3. $Z'$ Models

We follow the framework described in [11, 12] and explored in detail in [12]. Restricting the fermionic content to the three SM generations augmented just by three right-handed neutrinos and assuming that the $Z'$ couples universally to the three generations, a new $U(1)_X$ gauge group is constrained to act on the three fermion generations like an arbitrary linear combination of the SM hypercharge $Y$ and $B-L$, the difference of baryon and lepton number, as in equation (1).[11, 12] Our study is restricted to the case of a very heavy $Z'$ boson. Referring to the original, unmixed heavy gauge boson as $Z^{0\prime}$, we assume that the $Z^{0\prime}$ mass is generated primarily by a heavy SM-singlet Higgs boson $H'$ with a large vacuum expectation value, $v' \gg v = 246$ GeV, and that $m_{Z^{0\prime}} \gg m_Z^0$. In order to preserve the $U(1)_X$ gauge invariance of the SM Yukawa interactions, $Q_X$ must also act on the SM Higgs boson $H$ as indicated by equation (1). The interaction of $Z^{0\prime}$ with $H$ then gives rise to mass mixing between $Z^{0\prime}$ and the SM boson $Z^0$, resulting in the mass eigenstates $Z$ and $Z'$. In this framework $Z^0 - Z^{0\prime}$ mixing only occurs if $\theta_X \neq 0$.

The upper $2\times 2$ corner of the $3\times 3$ $W_3 - B - Z^{0\prime}$ mass matrix can be block diagonalized, yielding the massless photon eigenstate and the residual $2\times 2$ $Z^0 - Z^{0\prime}$ mass matrix, written compactly as

$$\mathcal{M}^2 = m_{Z^0}^2 \begin{pmatrix} 1 & -r\cos\theta_X \\ -r\cos\theta_X & \hat{m}_{Z^{0\prime}}^2 \end{pmatrix}. \tag{3}$$

In equation (3) $m_{Z^0} = g_Z v/2$ is the usual unmixed $Z^0$ boson mass, where $g_Z = g/\cos\theta_W$, $g$ is the $SU(2)_L$ gauge coupling constant, and $\theta_W$ is the weak interaction mixing angle. The quantity $r$ is the ratio of the $U(1)_X$ gauge coupling $g_{Z'}$ to $g_Z$,

$$r = \frac{g_{Z'}}{g_Z} \tag{4}$$

and $\hat{m}_{Z'}$ is the ratio of the $Z'$ mass to the $Z$ mass,

$$\hat{m}_{Z'} = \frac{m_{Z'}}{m_Z} \simeq \frac{m_{Z^{0\prime}}}{m_Z^0} \gg 1. \tag{5}$$

Diagonalizing the mass matrix the leading correction to the $Z$ boson mass is

$$\delta m_Z^2 = -r^2 \cos^2\theta_X \, \frac{m_Z^2}{\hat{m}_{Z'}^2} \tag{6}$$

and the $Z - Z'$ mixing angle $\theta_M$, defined by

$$Z = \cos\theta_M \, Z^0 + \sin\theta_M \, Z^{0\prime} \tag{7a}$$

$$Z' = \cos\theta_M \, Z^{0\prime} + \sin\theta_M \, Z^0, \tag{7b}$$

is

$$\theta_M = \frac{r\cos\theta_X}{\hat{m}_{Z'}^2}. \tag{8}$$

Per equation (5), equations (6) and (8) are correct to leading order in $1/\hat{m}_{Z'}^2$.

The effect of the shift in the $Z$ boson mass on the radiative corrections can be encoded[17] as a contribution to the oblique parameter $T$,[18]

$$\alpha T_X = -\frac{\delta m_Z^2}{m_Z^2} \tag{9}$$

so that

$$\alpha T_X = \frac{r^2\cos^2\theta_X}{\hat{m}_{Z'}^2}. \tag{10}$$

The negative sign in equation (6), that occurs because the "levels repel" in two body mixing, implies a positive sign for $T_X$, which then causes the EW fit to prefer larger values of the Higgs boson mass.

The second manifestation of $Z - Z'$ mixing on the radiative corrections is the shift in the $Z\overline{f}f$ couplings due to the admixture of $Z^{0\prime}$ in the $Z$ mass eigenstate. Including the oblique corrections the interaction is

$$\mathcal{L}_f = g_Z \left(1 + \frac{\alpha T_X}{2}\right) g_f' \overline{f} \not{Z} f \tag{11}$$

where $f$ represents a quark or lepton of chirality $L$ or $R$ and $g_f'$ encodes the $Z\overline{f}f$ coupling,

$$g_f' = g_f + r\theta_M q_X^f \tag{12}$$

Here $g_f$ is the SM $Z\overline{f}f$ coupling

$$g_f = t_{3L}^f - q^f \hat{x}_W \tag{13}$$

where $t_{3L}^f$ and $q^f$ are the weak isospin and electric charge of fermion $f$. The quantity $\hat{x}_W$ in equation (13) is the oblique-corrected square of the sin of the SM weak mixing angle, $x_W = \sin^2\theta_W$,

$$\hat{x}_W - x_W = -\frac{x_W(1-x_W)}{1-2x_W}\alpha T_X, \tag{14}$$

and $q_X^f$ is the $Q_X$ charge of fermion $f$,

$$q_X^f = \cos\theta_X \, \frac{y^f}{2} + \sin\theta_X \, \frac{b^f - l^f}{2} \tag{15}$$

where $y^f, b^f, l^f$ are respectively the weak hypercharge, baryon number, and lepton number of fermion $f$. In keeping with the approximation $\hat{m}_{Z'} \gg 1$ we kept only the leading term in $\theta_M$ in equation (12).

For a given choice of $\theta_X$ the effect of $Z - Z'$ mixing on the EW fit is determined by a single parameter, which we choose to be $T_X$. The shift in the $Z\overline{f}f$ coupling, equation (12) is determined by

$$\epsilon = r\,\theta_M, \tag{16}$$

which, using equations (8) and (10) is determined by $T_X$,

$$\epsilon = \frac{\alpha T_X}{\cos\theta_X}. \tag{17}$$

The $\chi^2$ fits presented in the section 5 are obtained by scanning over $T_X$ in addition to the four SM scanning parameters, $m_t, \Delta\alpha^{(5)}_{\rm had}(m_Z), \alpha_S(m_Z)$, and $m_H$. The value of $T_X$ determines the "effective Fermi constant" of the $Z'$ boson, defined as

$$G_{Z'} = \frac{g_{Z'}^2}{4\sqrt{2}\,m_{Z'}^2}. \tag{18}$$

Defining $G_Z$ analogously,

$$G_Z = \frac{g_Z^2}{4\sqrt{2}m_Z^2}, \tag{19}$$

which is equal at leading order to the Fermi constant, $G_Z = G_F$, we have

$$\hat{G}_{Z'} = \frac{G_{Z'}}{G_Z} = \frac{r^2}{\hat{m}_{Z'}^2} = \frac{\alpha T_X}{\cos^2\theta_X}. \tag{20}$$

Since $G_{Z'}$ is constrained by the LEP II bounds, for a given value of $\theta_X$ we obtain constraints on $T_X$ both from the EW fits and from the LEP II bounds.

Before proceeding to the EW fits of the $Z'$ models we briefly mention an amusing feature of the $Y$-sequential models. In general the EW corrections from $Z - Z'$ mixing include both an oblique correction $T_X$ from the shift in the $Z$ boson mass[17] and non-oblique corrections from shifts in the $Z\overline{f}f$ couplings, equation (12), due to the $Z^{0\prime}$ component of the $Z$ eigenstate. But for the case of a $Y$-sequential $Z'$ boson, $\theta_X = 0$, we find that both the oblique and non-oblique corrections can be fully parameterized by correlated "pseudo-oblique" parameters, $S'$ and $T'$, defined by

$$T' = -T_X \tag{21a}$$

$$S' = -4(1 - x_W)T_X \tag{21b}$$

where now

$$\alpha T_X = \epsilon = -\frac{\delta m_Z^2}{m_Z^2}. \tag{22}$$

The precision EW fit for the $Y$-sequential $Z'$ boson model can then be extracted from the usual oblique fit by considering the line $S = 4(1 - x_W)T$ in the $S, T$ plane with $T < 0$.

This parameterization of the model immediately reveals that the value of $m_H$ cannot be increased toward the TeV scale and into the domain of dynamical symmetry breaking, which requires positive $T$ and small or negative $S$.[6] Since the original model with $T_X > 0$ yields the same physics as the pseudo-oblique representation with $T' < 0$, because of the compensating effects of $\epsilon$ and $S'$, we also see that one cannot attach an absolute significance to the sign of weak isospin breaking.

The equivalence of the two representations is explained by the fact that for the $Y$-sequential model the apparently non-oblique correction to the $Z\overline{f}f$ couplings induces a rescaling of the SM hypercharge coupling constant, which in turn contributes to $W_3$-$B$ kinetic mixing parameterized by $S$. This is not true for the other models we consider with $\theta_X \neq 0$, since the term proportional to $B - L$ cannot be absorbed into a renormalization of any SM interaction. A derivation is presented in the Appendix.

## 4. Direct limits on $Z'$ bosons from LEP II and CDF

Carena *et al.*[8] have used LEP II bounds[9] on contact interactions to extract limits on a variety of $Z'$ bosons. Their results constrain the $Z'$ effective Fermi constant, that is, the ratio of $Z'$ mass to coupling strength, and in some cases they provide a stronger constraint than the precision EW data. For the interesting class of models with $0 \leq \theta_X < \pi/2$ the CDF collaboration has obtained bounds[10] which are stronger that the LEP II bounds if $g_{Z'}$ is sufficiently small, $g_{Z'} \lesssim g_Z/4$. Both direct and EW constraints are presented in the results presented below. In this section we summarize the LEP II and CDF constraints for the $Z'$ bosons considered in the EW fits presented in section 5 below.

The class of Abelian charges considered here, defined in equation (1), is equivalent, in the notation of Carena *et al.* to the group $U(1)_{q+xu}$, characterized by the parameter $x$ which ranges from $-\infty$ to $+\infty$ — see their table I. It is easy to see that the corresponding charge is

$$\hat{Q}_X = \frac{x-1}{3}Y + \frac{4-x}{3}(B - L) \tag{23}$$

so that their $x$ is related to our $\theta_X$ by

$$\tan\theta_X = \frac{4-x}{x-1}. \tag{24}$$

[6] See for instance figures (12) and (13) of the second paper cited in [2].

Defining $\hat{g}_{Z'}$ as the corresponding coupling constant, the relation between the coupling constants, determined by $\hat{g}_{Z'}\hat{Q}_X = g_{Z'}Q_X$, is

$$g_{Z'} = \frac{2}{3}\hat{g}_{Z'}\sqrt{2x^2 - 10x + 17}. \tag{25}$$

With this dictionary we can translate the bounds obtained in [8] to the notation used here. We will see below that the most interesting region in $\theta_X$ for the precision fits is the first quadrant, $0 \leq \theta_X < \pi/2$, corresponding to the interval $4 \geq x > 1$. Within this interval the 95% CL limit is (see figure 1 of [8])

$$\frac{m_{Z'}}{\hat{g}_{Z'}} > (2.62 + 1.18x)\text{TeV} \tag{26}$$

Using the dictionary, equations (24) and (25), and equations (4), (5), and (10), equation (26) implies a bound on $T_X$,

$$T_X \leq \frac{\alpha^{-1}(m_Z)}{(30.1 + 15.5\tan\theta_X)^2}, \tag{27}$$

valid for $0 < \theta_X \leq \pi/2$. However, it should be noted that for $\theta_X$ very near $\pi/2$ there must be a stronger bound, as can be seen by comparing the limits on $U(1)_{q+xu}$ and $U(1)_{B-xL}$ in figure 1 of [8]. At $x = 1$ both of these $U(1)$'s become $B - L$ but in the figure the latter is bounded more strongly than the former. A stronger bound must then exist on $Z'$ bosons with charge $Q_X$ for $\theta_X$ near $\pi/2$, that could be extracted from the two lepton differential cross sections, which are however not publicly available. In the following we restrict ourselves to the conservative bound, equation (27).[7]

Although the models with the greatest effect on $m_H$ lie in the first quadrant, $0 \leq \theta_X < \pi/2$, it is also interesting to consider the case $Q_X = T_{3R}$, since it occurs in attractive left-right extensions of the SM and also because it is typical of models in the second quadrant (or, equivalently, the fourth quadrant, since only the sign of $g_{Z'} \cdot Q_X$ is physical). For $Q_X = T_{3R}$ we have $\theta_X = -\pi/4$, which corresponds to $x \to \infty$ in the notation of [8]. The bound for this case is not discussed in [8], and we have extracted it directly from the LEP II constraint on the $RR$ contact interaction quoted in [9]. In addition to $T_{3R}$ we will sample the following choices from the first quadrant: $\theta_X = 0, \pi/6, \pi/3$, and $11\pi/24$, for which the LEP II bounds on $T_X$ and $\hat{G}_{Z'}$ are given in table 4.

The case of $\theta_X = 11\pi/24$ is interesting because we will see in the next section that it has an appreciable effect on the EW fit even though it is very near $\theta_X = \pi/2$ corresponding to $Q_X = B - L$, for which there is no $Z - Z'$ mixing and therefore no effect on the EW fit. However the surprisingly large effect that is found on the EW fit is severely constrained by the direct limit from equation (27) quoted in table 4.

| $\theta_X$ | $T_X$ | $\hat{G}_{Z'}$ |
|---|---|---|
| 0 | 0.14 | 0.0011 |
| $\pi/6$ | 0.084 | 0.00088 |
| $\pi/3$ | 0.039 | 0.0012 |
| $11\pi/24$ | 0.0059 | 0.0027 |
| $-\pi/4$ | 0.30 | 0.0047 |

Table 4: 95% CL upper limits on $T_X$ and $\hat{G}_{Z'}$ obtained from LEP II bounds on contact interactions.

| $\theta_X$ | r | $m_{Z'}$ (TeV) | $T_X$ |
|---|---|---|---|
| | 0.27 | 0.83 | 0.11 |
| 0 | 0.13 | 0.70 | 0.039 |
| | 0.081 | 0.61 | 0.019 |
| | 0.20 | 0.78 | 0.051 |
| $\pi/6$ | 0.098 | 0.64 | 0.019 |
| | 0.059 | 0.54 | 0.0095 |
| | 0.20 | 0.75 | 0.018 |
| $\pi/3$ | 0.098 | 0.60 | 0.0070 |
| | 0.059 | 0.45 | 0.0046 |
| | 0.24 | 0.69 | 0.0022 |
| $11\pi/24$ | 0.12 | 0.50 | 0.0010 |
| | 0.072 | 0.40 | 0.00058 |

Table 5: 95% CL upper limits on $T_X$ and $m_{Z'}$ from CDF[10] for given values of $r = g_{Z'}/g_Z$.

The corresponding bounds on $T_X$ from the CDF collaboration[10] are given in table 5, translated from the notation of reference [8], which is followed in reference [10], to the notation used here. For each $\theta_X$ in table 4, except $\theta_X = -\pi/4$ for which no bound is given by CDF, we present the implied limit on $m_{Z'}$ and $T_X$ for given values of the $Z'$ coupling strength, parameterized as the ratio to the SM $Z$ boson coupling, $r = g_{Z'}/g_Z$. Comparing tables 4 and 5, we see that the CDF bounds are stronger than the LEP II bounds for $r \lesssim 1/4$, becoming increasingly stronger as $r$ decreases. The LEP II bounds depend only on the ratio $g_{Z'}/m_{Z'}$, i.e., on the effective Fermi constant $G_{Z'}$, independent of the value of $g_{Z'}$, because with $m_{Z'} \gg m_Z$ they arise purely from the interference of the high energy tail of the $Z$ boson amplitude with the low energy tail of the $Z'$ amplitude. At Fermilab for sufficiently small $g_{Z'}$, which corresponds to smaller $m_{Z'}$ for fixed $G_{Z'}$, the data begins to be sensitive to the direct production term, i.e., the square of the $Z'$ amplitude, giving rise to increased sensitivity and a stronger constraint.

## 5. Electroweak Fits in $Z'$ Models

In this section we present fits to the precision EW data for the class of $Z'$ models discussed in section 3, focusing on the effect of $Z - Z'$ mixing on the value of the Higgs boson mass obtained from the fits. We will use two statistical methods that illuminate the physics in different ways, because they answer questions that are different in detail though they are clearly related. The first is the classical frequentist method, which is used by the EWWG[1] and was used in the discussion of the SM fit in section 2. In this method the question is 'Without imposing any *a priori* knowledge, direct or indirect, of the value of $m_H$, how well does the model describe the precision data and what prediction does the best fit make for the likelihood of different values of $m_H$?' The second approach, followed for instance in the analysis of $Z'$ models in [6], might be termed "Bayesian," in the sense that it imposes external knowledge about $m_H$ as a "prior" constraint on the fit and therefore assesses the extent to which the fit of the model to the precision EW data is consistent with that prior. This approach then answers a different question which might be stated as follows: 'If the value of $m_H$ were known to have a specific value or to lie within a certain range, how well does the model fit the precision data?'

Both questions are valid and interesting, and it is useful to see what each tells us about the compatibility of various values of $m_H$ with the different models. We will consider each in turn, combining the constraints from the fits with the direct LEP II bounds on $Z'$ bosons in table 4.

### *5a. Frequentist Fits*

We first present the frequentist fits for the models listed in table 4. These fits contain

[7] I thank the authors of [8] for correspondence on this point.

| Data Set | $\chi^2/N$ | CL | $m_H$ (GeV) | $m_H(95\%)$ | CL($m_H > 114$) |
|---|---|---|---|---|---|
| **A** | 16.5/11 | 0.12 | 85 | 153 | 0.24 |
| **B** | 5.63/9 | 0.78 | 50 | 105 | 0.03 |

Table 6: SM fits A and B. $m_H(95\%)$ is the usual frequentist 95% upper limit on $m_H$ .

one more free parameter than the SM fits, which may be chosen to be the effective Fermi constant $G_{Z'}$ or equivalently $T_X$ (see equation (20)). In the frequentist approach to the SM fits, the global $\chi^2$ minimum is determined by freely varying $m_t, \Delta\alpha^{(5)}_{\rm had}(m_Z), \alpha_S(m_Z)$, and $m_H$. The 95% CL upper limit on $m_H$ is then determined by minimizing $\chi^2$ as $m_H$ is varied away from its value at the global minimum, until the local $\chi^2$ minimum (i.e., for the given value of $m_H$) has increased by $\Delta\chi^2 = 2.71$, corresponding to the upper boundary of the symmetric 90% confidence interval for one degree of freedom, $CL(2.71, 1) = 0.90$.

To extend this approach to the $Z'$ models, we vary $T_X$ in addition to $m_t, \Delta\alpha^{(5)}_{\rm had}(m_Z)$, $\alpha_S(m_Z)$, and $m_H$, to obtain the global $\chi^2$ minimum, reducing the number of degrees of freedom by one relative to the SM fit, and then vary both $T_X$ and $m_H$ about the $\chi^2$ minimum. The 90% contour in the $m_H - T_X$ plane is then defined by $\Delta\chi^2 = 4.61$ corresponding to $CL(4.61, 2) = 0.90$, and similarly the 95% contour is at $\Delta\chi^2 = 5.99$. The allowed regions are then further constrained by the 95% exclusion limits on $T_X$ from the LEP II bounds on contact interactions, table 4, which are superimposed over the contours from the precision data.

We consider two data sets. Data set B excludes the three hadronic asymmetry measurements. Set A contains all of the measurements in table 1 except the jet charge asymmetry, $Q_{FB}$, which we omit for simplicity. (To compute the correction to $Q_{FB}$ we would have to convolute the mixing-induced shifts in the $Z\overline{q}q$ couplings with the $\overline{q}q$ partial rates, and then unfold the result to obtain the effective value of $\sin^2\theta_W^{\ell\ \rm eff}$.) $Q_{FB}$ has very little impact on the fit CL or on $m_H$: figure 2 shows that $A^b_{FB}$ completely dominates $A^c_{FB}$ and $Q_{FB}$ in the $\chi^2$ distribution, since the combined distribution is practically indistinguishable from the distribution of $A^b_{FB}$ alone.

The SM fits to data sets A and B are summarized in table 6. $m_H(95\%)$ is the frequentist 95% CL upper limit, at $\chi^2 = \chi^2_{\rm MIN} + 2.71$. Fit A has an acceptable prediction for $m_H$ but a marginal confidence level, while fit B has a robust $\chi^2$ CL but a failed prediction for $m_H$. The $Z - Z'$ model fits to data sets A and B are shown in table 7 and figures 3 - 7. The effect of $Z - Z'$ mixing on data set A is to push $A^b_{FB}$ further from the experimental value than the $2.82\sigma$ deviation of the SM fit, so that the minima for set A coincide with the SM and

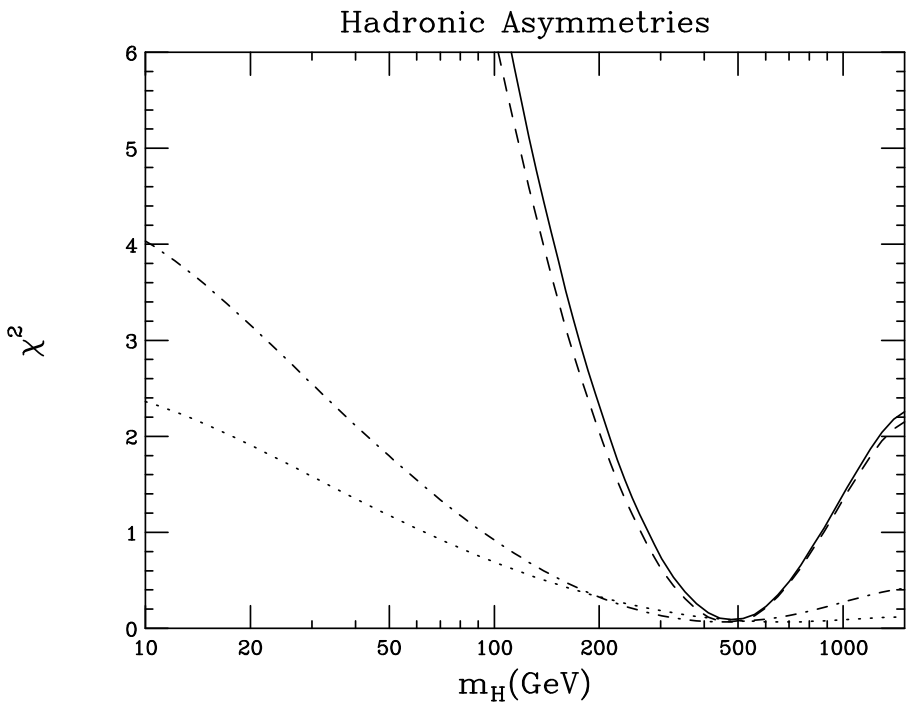


Figure 2: $\chi^2$ distributions as a function of $m_H$ for the combination of the three hadronic asymmetry measurements (solid line) and for each individually: $A^b_{FB}$ (dashes), $A^c_{FB}$ (dashdot), and $Q_{FB}$ (dots).

$\chi^2$ increases rapidly away from the SM minimum. As shown in table 7, the $\chi^2$ minimum for data set A is then at $T_X = 0$ for all values of $\theta_X$, implying zero mixing, $\theta_M = 0$. The $\chi^2$ value and the central value of $m_H$ are then identical to the SM fit, while the confidence level decreases since there is one fewer degree of freedom, from CL(16.5,11) = 0.12 to CL(16.5,10) = 0.09. For set B the fits favor nonzero but small mixing for models with $\theta_X$ in the first quadrant, with modest decreases in the $\chi^2$ minimum and modest increases in $m_H$, while the fit likelihoods decrease slightly. For $T_{3R}$ as for all models with $\theta_X$ in the second quadrant, the $\chi^2$ minimum is at zero $Z - Z'$ mixing, except for $\theta_X$ very near $\pi$ where $Q_X \simeq Y$.[8]

Although the changes in the $\chi^2$ minima are modest at best, there is a substantial effect on the allowed range of Higgs boson masses in the case of data set B and a smaller effect for data set A. This can be seen in the 90 and 95% contours shown in figures 3 - 7. For the $Y$-sequential model, $\theta_X = 0$, in the case of data set B the 90% contour extends to $m_H = 260$ GeV, a factor 2.5 beyond the 105 GeV 95% upper limit of the SM fit.[9] The

[8]Note that quadrants I and III in $\theta_X$ are physically equivalent, as are quadrants II and IV, since the overall phase of $Q_X$ is not physical because it can be compensated by the phase of $g_{Z'}$.

[9]The 90% contour of the $Z - Z'$ fit should be compared to the symmetric 90% confidence interval of the SM fit, whose upper boundary defines the 95% upper limit. The extreme of the 95% contour corresponds to the 97.5% upper limit of the SM fit.

| | Data Set A | | | | Data Set B | | | |
|---|---|---|---|---|---|---|---|---|
| $\theta_X$ | $\chi^2/N$ | CL | $m_H$ (GeV) | $T_X$ | $\chi^2/N$ | CL | $m_H$ (GeV) | $T_X$ |
| 0 | 16.5/10 | 0.09 | 85 | 0.0 | 5.56/8 | 0.70 | 61 | 0.012 |
| $\pi/6$ | 16.5/10 | 0.09 | 85 | 0.0 | 5.39/8 | 0.72 | 70 | 0.019 |
| $\pi/3$ | 16.5/10 | 0.09 | 85 | 0.0 | 5.22/8 | 0.73 | 70 | 0.014 |
| $11\pi/24$ | 16.5/10 | 0.09 | 85 | 0.0 | 5.00/8 | 0.76 | 70 | 0.006 |
| $-\pi/4$ | 16.5/10 | 0.09 | 85 | 0.0 | 5.63/8 | 0.69 | 50 | 0.0 |

Table 7: Frequentist $\chi^2$ fits for $Z'$ models.

LEP II upper limit from table 4, $T_X < 0.14$, does not impinge on the contours from the EW fit. The maximum reach in $m_H$ occurs at $T_X = 0.10$, corresponding to $\hat{G}_{Z'} \simeq 8 \cdot 10^{-4}$; if the $Z'$ coupling were of electroweak strength, this would imply a mass hierarchy of order $m_{Z'}/m_Z \simeq 30$ or $m_{Z'} \simeq 3$ TeV, within the range of the LHC. For fit A the increase in $m_H$ is smaller, with the extreme of the 90% contour reaching 230 GeV, a factor 1.5 above the SM 95% upper limit at 153 GeV. Although the SM fit of data set B predict smaller values of $m_H$ than set A, with $Z - Z'$ mixing set B is consistent with larger values than set A.

Figures 4 and 5 show that these features persist for $\theta_X = \pi/6$ and $\pi/3$. The LEP II constraint on $G_{Z'}$ begins to limit the allowed region for data set B, both because the LEP II bound becomes stronger and also because as $\theta_X$ increases toward $\pi/2$ the ratio of $G_{Z'}$ to $T_X$ increases like $1/\cos^2\theta_X$, as seen in equation (20). Even though $\theta_X = 11\pi/24$ is very near $\pi/2$, $Q_X = B - L$, for which there is no mixing and no effect on the fits, there is still a significant effect on the allowed region in $m_H$ for data set B, shown in figure 6. However, the allowed range is severely constricted by the direct limit on $G_{Z'}$, which, as discussed in section 4, is likely to be even stronger than is shown in the figure. For $Q_X = T_{3R}$ the effect of $Z - Z'$ mixing on $m_H$ is weaker, as can be seen from the more vertical slopes of the contour lines above 114 GeV in figure 7, but there is no additional constraint from the LEP II upper limit on $G_{Z'}$ which is $T_X > 0.30$.

To estimate the confidence levels for these fits to lie within the LEP II allowed regions for $m_H$ and $G_{Z'}$ we use a Bayesian likelihood method that was developed in the second paper cited in [2] to compute CL($m_H > 114$GeV) for the SM fits. In that approach two Bayesian priors were introduced to convert unnormalized likelihood functions into normalized probability distributions from which confidence intervals could be extracted. The first prior is that $m_H$ lies between 10 and 3000 GeV. The precise value of the limits is not critical since there is negligible support above 1000 GeV or below 10 GeV. The second prior is that $\log m_H$ is the appropriate measure, a natural assumption since the EW corrections depend

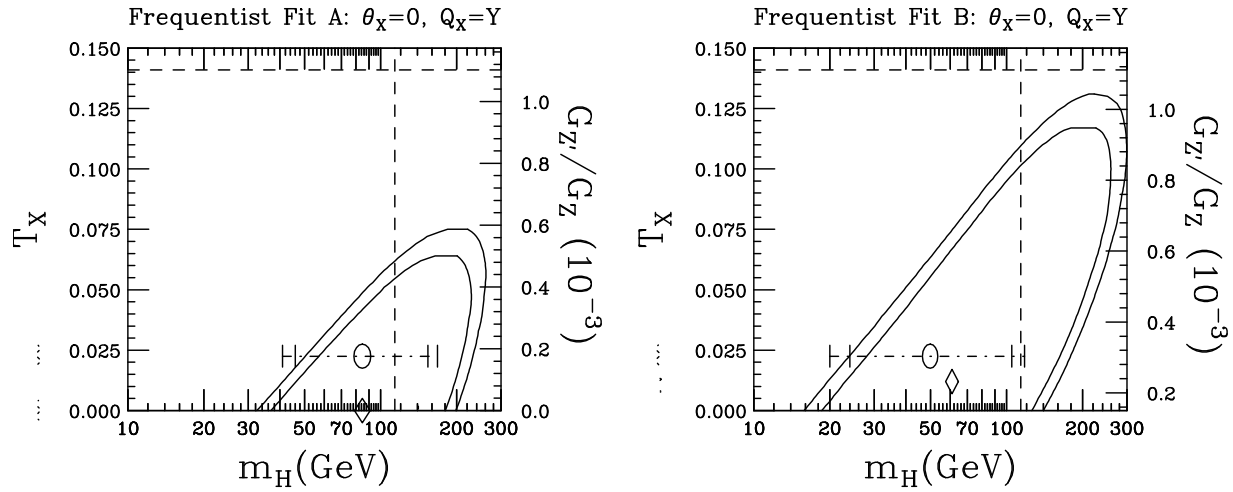


Figure 3: 90% and 95% CL contours in the $T_X - m_H$ plane for frequentist fits to data sets A and B for the $Y$-sequential model, $\theta_X = 0$. The right axis indicates the corresponding values of $\hat{G}_{Z'} = G_{Z'}/G_Z$ per equation (20). The diamond indicates $m_H, T_X$ at the $\chi^2$ minimum for the $Z'$ model. (Note that for set A for all $\theta_X$ the $\chi^2$ minimum is at $T_X = 0$ and the diamond is hiding on the x-axis.) The ellipse and dot-dash horizontal line display the central value and 90, 95% symmetric confidence intervals of $m_H$ for the SM fit (elevated above $T_X = 0$ only for clarity). The horizontal dashed line is the 95% CL upper limit on $\hat{G}_{Z'}$ extracted from LEP II data. The vertical dashed line is the LEP II 95% lower limit on $m_H$.

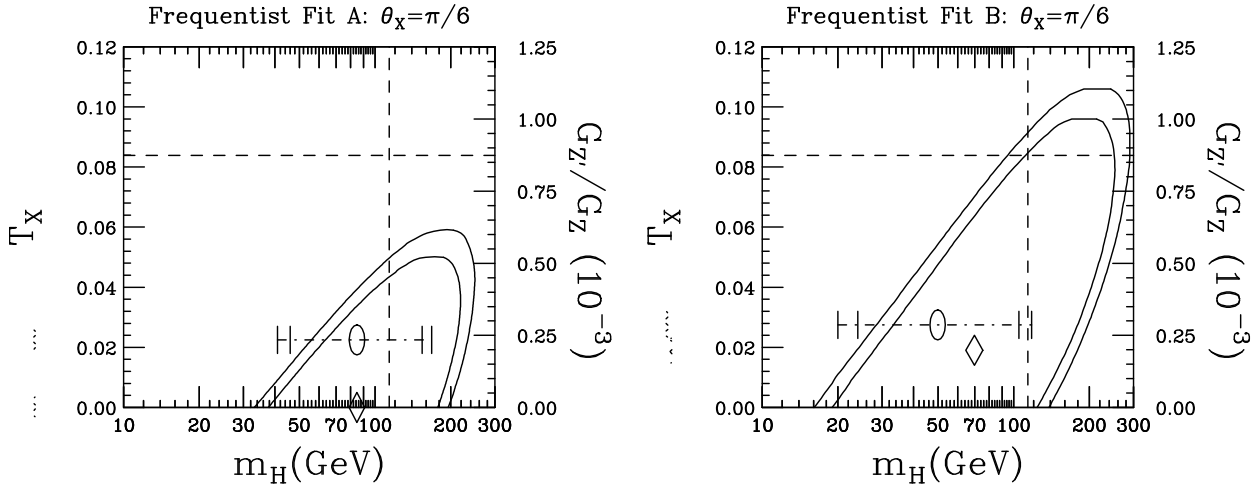


Figure 4: 90% and 95% CL frequentist contours for $Z'$ model with $\theta_X = \pi/6$, as in figure 3.

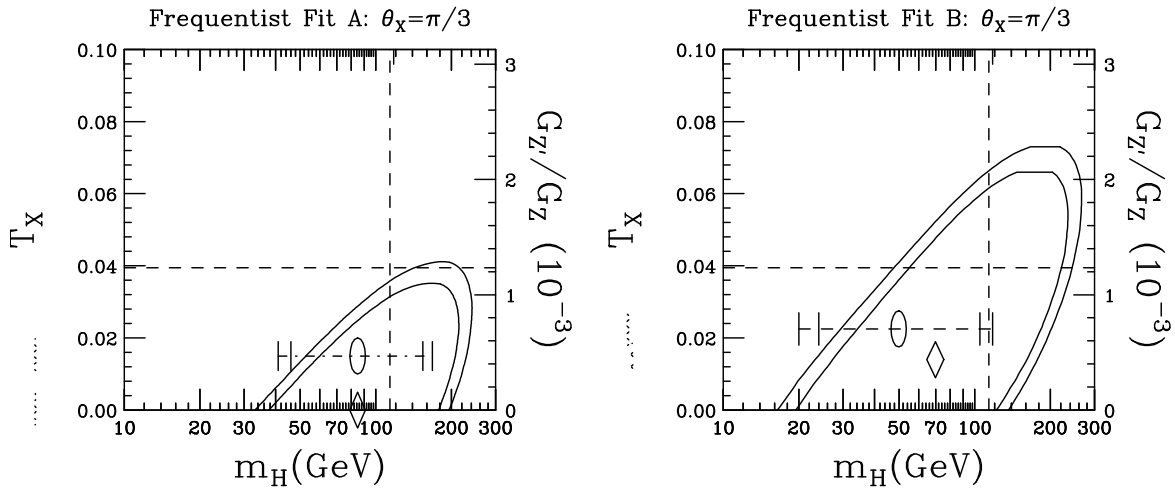


Figure 5: 90% and 95% CL frequentist contours for $Z'$ model with $\theta_X = \pi/3$, as in figure 3.

logarithmically on $m_H$.

This procedure was shown to be reasonable (or at least no more foolish than the conventional procedure) by the fact that it provided confidence intervals for $m_H$ similar to those obtained from the $\Delta\chi^2$ method, e.g., for data set B the result was CL($m_H > 114$) = 0.030 from the Bayesian likelihood method versus 0.035 from $\Delta\chi^2$ with the data of the time. We now find CL($m_H > 114$) = 0.17 from the SM fit to data set A compared to 0.24 from $\Delta\chi^2$, and 0.018 compared to 0.031 for set B. There is no reason that the two methods should agree precisely. An important difference is that the $\Delta\chi^2$ method compares only the *best* fits at different values of $m_H$, while the Bayesian likelihood method samples the complete distribution of scanned parameters $(m_t, \Delta\alpha_5, \alpha_S)$ at each value of $m_H$.

The same method can be applied to the two dimensional distributions in $m_H$ and $T_X$. The natural measure for $m_H$ is again logarithmic. Since $T_X$ represents a first order perturbation of new physics on the leading order SM, the natural measure for $T_X$ is linear. We normalize the likelihood functions in the intervals $0 < T_X < 0.25$ and $10 < m_H < 3000$ GeV, where again the results are insensitive to to the precise choice of limits.[10] The results are tabulated in table 8, which displays the confidence levels for $m_H > 114$ GeV, both without and with the LEP II constraint on $T_X$. In addition we tabulate $m_H(95\%)$, which for the $Z'$ models is defined as the largest value of $m_H$ on the 90% contour that is consistent with the LEP II bound on $G_{Z'}$. Unlike $m_H(95\%)$ for the SM fits, the values quoted for the $Z'$ models cannot be interpreted as reflecting a 5% probability for $m_H > m_H(95\%)$. Again the impact of $Z - Z'$ mixing is greater for data set B, with the probability of the LEP II allowed regions increasing by an order of magnitude relative to the SM value, e.g., from

[10] $T_X > 0$ is a boundary condition imposed by $Z - Z'$ mixing.

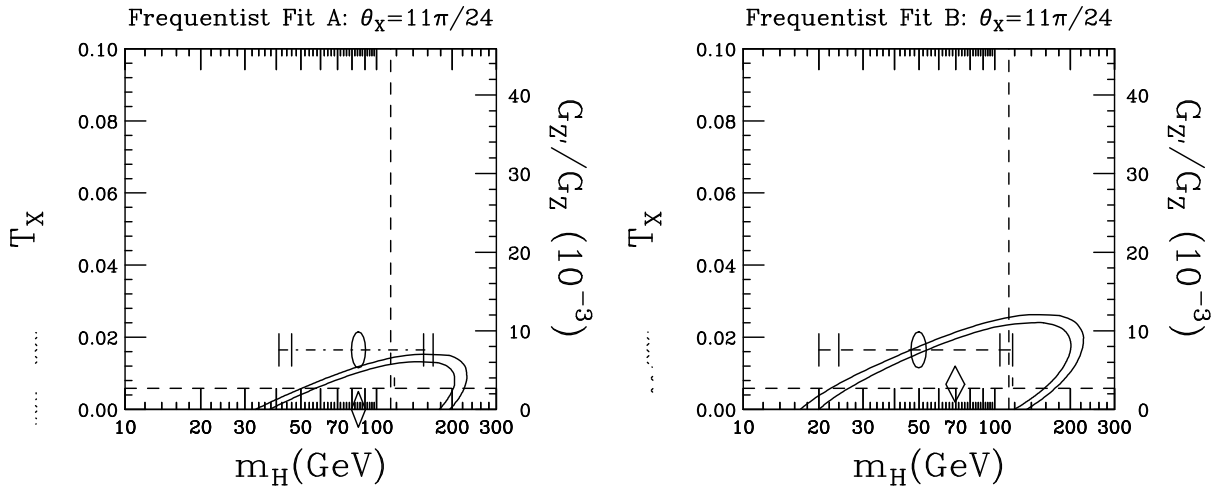


Figure 6: 90% and 95% CL frequentist contours for $Z'$ model with $\theta_X = 11\pi/24$, as in figure 3.

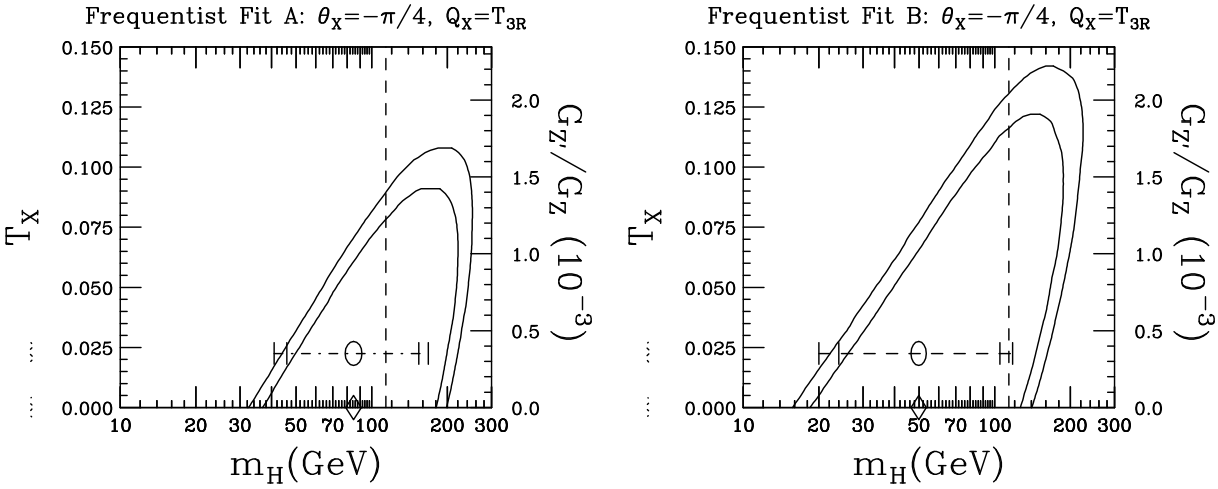


Figure 7: 90% and 95% CL frequentist contours for $Z'$ model with $\theta_X = -\pi/4$, $Q_X = T_{3R}$, as in figure 3. The LEP II upper limit, $T_X < 0.30$, is off the graph.

| Data Set | Model | $m_H(95\%)$ | CL($m_H > 114$) | **and** CL($T_X > T_{\text{LEP II}}$) |
|---|---|---|---|---|
| **A** | SM | 153 | 0.17 | ... |
| | $\theta_X = 0$ | 230 | 0.44 | 0.44 |
| | $\pi/6$ | 220 | 0.42 | 0.42 |
| | $\pi/3$ | 214 | 0.39 | 0.38 |
| | $11\pi/24$ | 202 | 0.34 | 0.15 |
| | $-\pi/4$ | 220 | 0.43 | 0.43 |
| **B** | SM | 105 | 0.018 | ... |
| | $\theta_X = 0$ | 260 | 0.29 | 0.29 |
| | $\pi/6$ | 252 | 0.28 | 0.24 |
| | $\pi/3$ | 221 | 0.23 | 0.12 |
| | $11\pi/24$ | 158 | 0.14 | 0.01 |
| | $-\pi/4$ | 188 | 0.18 | 0.18 |

Table 8: Fits of data sets A and B. For the SM $m_H(95\%)$ is the usual 95% upper limit obtained by the $\Delta\chi^2$ method. For the $Z'$ models $m_H(95\%)$ is the maximum value of $m_H$ on the 90% frequentist contours (figures 3 - 7) that is consistent with the LEP II direct limit on $T_X$. The confidence levels CL($m_H > 114$) and CL($T_X > T_{\text{LEP II}}$) are computed with the Bayesian likelihood method described in the text. The entries in the last column combine both the $m_H$ and $T_X$ direct limits from LEP II.

| Model | r | Data Set A | | Data Set B | |
|---|---|---|---|---|---|
| | | $m_H(95\%)$ CDF | $m_H(95\%)$ LEP II | $m_H(95\%)$ CDF | $m_H(95\%)$ LEP II |
| | 0.27 | 230 | | 260 | |
| $\theta_X = 0$ | 0.13 | 225 | 230 | 190 | 260 |
| | 0.081 | 206 | | 139 | |
| | 0.20 | 220 | | 224 | |
| $\pi/6$ | 0.098 | 207 | 220 | 163 | 252 |
| | 0.059 | 194 | | 143 | |
| | 0.20 | 214 | | 172 | |
| $\pi/3$ | 0.098 | 193 | 214 | 141 | 221 |
| | 0.059 | 188 | | 134 | |
| | 0.24 | 188 | | 134 | |
| $11\pi/24$ | 0.12 | 183 | 202 | 127 | 158 |
| | 0.072 | 181 | | 124 | |

Table 9: Effect of CDF bounds on the Higgs boson mass from frequentist fits of data sets A and B. As in table 8, $m_H(95\%)$ is the maximum value of $m_H$ on the 90% frequentist contours (figures 3 - 7) that is consistent with the CDF direct limit on $T_X$ for given values of $r = g_Z/g_{Z'}$. The values of $m_H(95\%)$ required by the LEP II bounds on $T_X$, which are independent of $r$, are shown for comparison.

CL($m_H > 114$) = 0.018 for the SM to 0.29 for the $Y$-sequential model.

In table 9 we show the effect of the CDF constraints from table 5 on the frequentist fits of data sets A and B. In particular for each value of $r = g_{Z'}/g_Z$ we display $m_H(95\%)$, defined as in table 8, as the largest value of $m_H$ on the 90% contours (figures 3 - 7) consistent with the corresponding upper limit on $T_X$ from table 5. There is no CDF constraint for $Q_X = T_3R$.

*5b. Bayesian Fits*

In the frequentist fits presented above we scanned over $m_H$ as a free parameter, with no prior assumption except the exceedingly mild prior, $10 < m_H < 3000$ GeV, that was used only to obtain the confidence levels in table 8 for the regions in the $m_H, T_X$ plane allowed by the direct LEP II limits on $m_H$ and $G_{Z'}$. The EW precision data alone determines the outcomes of those fits, which make predictions about the value of $m_H$ that can be tested for consistency with the direct LEP II lower bound on $m_H$. In this section we follow a different procedure: we suppose that the Higgs boson has been discovered at a specific mass which is

imposed as a prior constraint on the fits and ask how well the models describe the precision data for that value of $m_H$. This is the approach followed in [6]. We refer to this procedure as Bayesian because it assumes a prior value for $m_H$.

In table 10 we present results for $m_H = 114, 225$, and 300 GeV. Since $m_H$ is fixed these fits have one more degree of freedom than the corresponding fits in section 5a. For each fit we present the minimum $\chi^2$, the corresponding confidence level, the change in $\chi^2$ relative to the SM, and the value of $T_X$ at the $\chi^2$ minimum. When $T_X$ at the $\chi^2$ minimum exceeds the LEP II limit tabulated in table 4, we instead evaluate the fit with $T_X$ set to the limit (marked by asterisks in table 10), so that the quoted $\chi^2$ is then the smallest value consistent with the LEP II limit.

For data set A the Bayesian $Z'$ fits at $m_H = 114$ GeV do not improve on the SM fit, and the confidence levels are lower than the SM CL. For $m_H = 225$ and 300 GeV the $Z'$ fits of set A have larger CL's than SM fit but they are still unacceptably low, $\lesssim 0.03$ and $\lesssim 0.01$ respectively. For data set B the $Z'$ models have a greater effect on the fits, and in all cases they improve on the SM. For $m_H = 225$ and 300 GeV the confidence levels of the $Z'$ fits are larger than the SM CL's by one and two orders of magnitude respectively, and the $\Delta\chi^2$ values are highly significant. The $Z'$ fit for $\theta_X = 11\pi/24$ is severely constrained by the strong LEP II limit on $T_X$. The $Z'$ models with the greatest effect on the fits are in the range $0 \lesssim \theta_X \lesssim \pi/3$, with the effect for $\theta_X \simeq \pi/3$ restricted by the LEP II limit on $T_X$ for the larger values of $m_H$. For $0 \lesssim \theta_X \lesssim \pi/6$ the confidence levels are quite acceptable all the way up to $m_H = 300$ GeV. The large values of $\Delta\chi^2$ in table 10 are unambiguous evidence of the effectiveness of the $Z'$ model for set B with $m_H = 225$ and 300 GeV.

Contour plots for these Bayesian $\chi^2$ fits are shown in figures 8 - 12. For the $Z'$ models we exhibit the 90% and 95% contours with the LEP II limits on $m_H$ and $T_X$ superimposed. The 90 and 95% confidence intervals for the corresponding SM fits are indicated by the tick marks on the horizontal dot-dashed line, elevated above the x-axis for visibility. With the Bayesian prescription, these intervals mark the value of $m_H$ at which $\mathrm{CL}(\chi^2/N) = 0.10$ or 0.05, with $N = 12$ for the SM fit to set A and $N = 10$ for B. Similarly the $Z'$ contour plots are the 90 and 95% trajectories in the ($m_H$, $T_X$) plane with $N = 11$ and 9 for A and B respectively. Table 11 presents 95% upper limits on $m_H$ from these fits, defined for the SM as the upper limit of the 90% symmetric Bayesian confidence interval and for the $Z'$ models as the largest value of $m_H$ on the 90% contour that is consistent with the LEP II limit on $T_X$. For data set A the 95% upper limits of the $Z'$ models are lower than for the SM, while for set B the limits increases relative to the SM, by a factor $\simeq 2$ to nearly 400 GeV for the $Y$-sequential boson. A qualitatively similar conclusion was reached by Ferroglia *et al.*,[6] who used the statistical method that we refer to here as Bayesian.

It is interesting to reflect on the differences in the $m_H$ confidence intervals for the fre-

| | | Data Set A | | | | Data Set B | | | |
|---|---|---|---|---|---|---|---|---|---|
| $m_H$ | Model | $\chi^2/N$ | $T_X$ | CL | $\Delta\chi^2$ | $\chi^2/N$ | $T_X$ | CL | $\Delta\chi^2$ |
| 114 | SM | 17.0/12 | ... | 0.15 | ... | 9.10/10 | ... | 0.52 | ... |
| | $\theta_X = 0$ | 17.0/11 | 0.003 | 0.11 | 0.0 | 6.15/9 | 0.043 | 0.72 | 2.96 |
| | $\pi/6$ | 17.0/11 | 0.003 | 0.11 | 0.0 | 5.87/9 | 0.037 | 0.75 | 3.24 |
| | $\pi/3$ | 17.0/11 | 0.002 | 0.11 | 0.0 | 5.72/9 | 0.027 | 0.77 | 3.39 |
| | $11\pi/24$ | 17.0/11 | 0.001 | 0.11 | 0.0 | 6.32/9 | 0.0059* | 0.71 | 2.79 |
| | $-\pi/4$ | 17.0/11 | 0.003 | 0.11 | 0.0 | 7.48/9 | 0.045 | 0.59 | 1.63 |
| 225 | SM | 25.0/12 | ... | 0.015 | ... | 20.5/10 | ... | 0.025 | ... |
| | $\theta_X = 0$ | 21.2/11 | 0.047 | 0.031 | 3.8 | 9.0/9 | 0.089 | 0.44 | 11.5 |
| | $\pi/6$ | 21.4/11 | 0.038 | 0.029 | 3.6 | 9.0/9 | 0.073 | 0.43 | 11.5 |
| | $\pi/3$ | 21.7/11 | 0.025 | 0.027 | 3.3 | 10.0/9 | 0.039* | 0.35 | 10.5 |
| | $11\pi/24$ | 22.5/11 | 0.0059* | .021 | 2.5 | 13.4/9 | 0.0059* | 0.15 | 7.1 |
| | $-\pi/4$ | 21.6/11 | 0.068 | 0.028 | 3.4 | 11.6/9 | 0.12 | 0.23 | 8.9 |
| 300 | SM | 31.8/12 | ... | 0.0015 | ... | 28.7/10 | ... | 0.0014 | ... |
| | $\theta_X = 0$ | 24.6/11 | 0.062 | 0.01 | 7.2 | 11.7/9 | 0.11 | 0.23 | 17.0 |
| | $\pi/6$ | 24.9/11 | 0.054 | 0.01 | 6.9 | 11.8/9 | 0.084* | 0.22 | 16.9 |
| | $\pi/3$ | 25.5/11 | 0.025 | 0.008 | 6.3 | 14.7/9 | 0.039* | 0.10 | 14.0 |
| | $11\pi/24$ | 27.8/11 | 0.0059* | 0.003 | 4.0 | 22.0/9 | 0.0059* | 0.01 | 6.7 |
| | $-\pi/4$ | 24.8/11 | 0.10 | 0.01 | 7.0 | 14.9/9 | 0.15 | 0.09 | 13.8 |

Table 10: Bayesian fits of data sets A and B assuming fixed values of $m_H$ at 114, 225, and 300 GeV. $\chi^2$ is the chi-square minimum and $N$ is the number of degrees of freedom. $T_X$ is the value at the $\chi^2$ minimum unless it exceeds the LEP II limit in table 4, in which case the fit is evaluated at the LEP II limit, denoted by an asterix. CL is the $\chi^2$ confidence level and $\Delta\chi^2$ is the $\chi^2$ difference between the $Z'$ model and the SM fit.

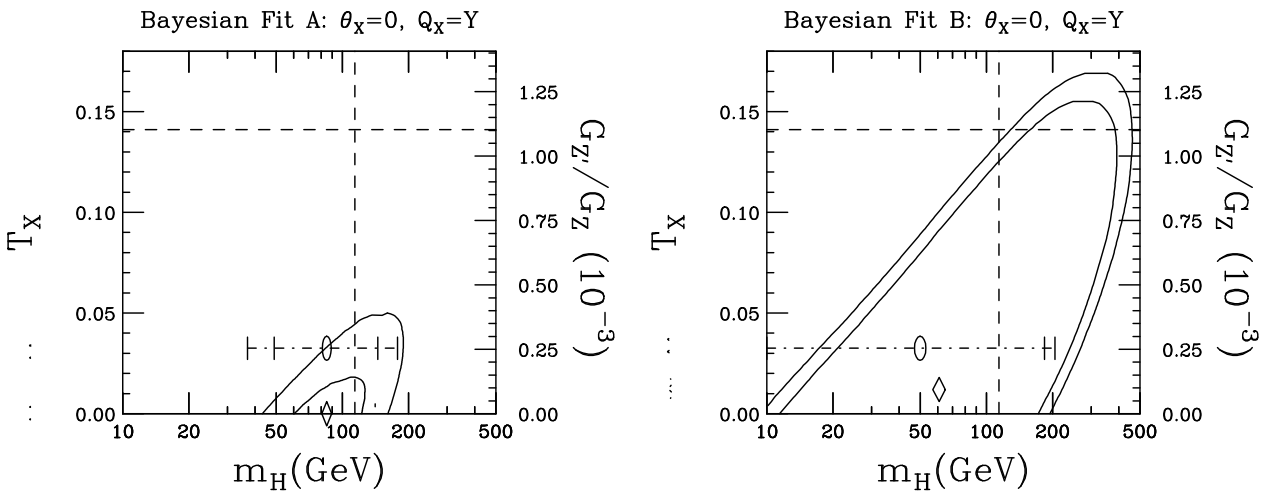


Figure 8: 90% and 95% CL contours in the $T_X - m_H$ plane for Bayesian fits, as defined in the text, to data sets A and B for the $Y$-sequential model, $\theta_X = 0$. The right axis indicates the corresponding values of $\hat{G}_{Z'} = G_{Z'}/G_Z$ per equation (20). The diamond indicates $m_H, T_X$ at the $\chi^2$ minimum for the $Z'$ model. (Note that for set A for all $\theta_X$ the $\chi^2$ minimum is at $T_X = 0$ and the diamond is hiding on the x-axis.) The ellipse and dot-dash horizontal line display the central value and 90, 95% symmetric (Bayesian) confidence intervals of $m_H$ for the SM fit (elevated above $T_X = 0$ only for clarity). The horizontal dashed line is the 95% CL upper limit on $T_X$ extracted from LEP II data. The vertical dashed line is the LEP II 95% lower limit on $m_H$.

quentist and Bayesian fits of data sets A and B. Consider first the SM fits. In the frequentist fits the 95% upper limit for $m_H$ (the maximum of the 90% symmetric confidence interval) is 153 GeV for set A and 105 GeV for set B, while for the Bayesian fits the pattern is reversed with 143 GeV for A and 183 GeV for B. The difference is due to the smaller confidence level of the fits to set A, e.g., $\mathrm{CL}(16.54, 12) = 0.13$ for the frequentist fit to set A, compared to $\mathrm{CL}(5.63, 9) = 0.78$ for B. The greater reach in $m_H$ of the Bayesian SM fit to set B is a consequence of the higher confidence level of the fit at the $\chi^2$ minimum, which allows for a greater excursion in $m_H$, even though $m_H$ at the $\chi^2$ minimum is smaller for B than for A. In the frequentist fits the $\Delta\chi^2$ method is used to compute the confidence intervals. In that method one computes the change in $\chi^2$ from the $\chi^2$ minimum, without regard to what the value of $\chi^2$ actually is at the minimum, so there is no penalty for the larger $\chi^2$ minimum of set A, and the 90% interval reaches to larger $m_H$ because of the influence of the hadronic asymmetries. In a sense the $\Delta\chi^2$ method is Bayesian, since it assumes the fit at the $\chi^2$ minimum as a prior and then estimates the likelihood for deviations from the minimum.

For data set A with $m_H$ near 114 GeV the $\chi^2$ minima occur at very small values of $T_X$, as can be seen in table 10. The resulting fits have essentially the same $\chi^2$ minima as the SM

| Model | Data Set A $m_H(95\%)$ | Data Set A $T_X$ | Data Set B $m_H(95\%)$ | Data Set B $T_X$ |
|---|---|---|---|---|
| SM | 143 GeV | ... | 183 GeV | ... |
| $\theta_X = 0$ | 127 | 0.01 | 390 | 0.13 |
| $\pi/6$ | 128 | 0.01 | 368 | 0.084* |
| $\pi/3$ | 128 | 0.007 | 300 | 0.039* |
| $11\pi/24$ | 128 | 0.003 | 220 | 0.0059* |
| $-\pi/4$ | 124 | 0.01 | 300 | 0.13 |

Table 11: 95% upper limits on $m_H$ with the corresponding value of $T_X$, from the Bayesian fits. $m_H(95\%)$ is defined as the largest value of $m_H$ on the 90% Bayesian contours (figures 8 - 12) consistent with the LEP II upper limit on $T_X$. An asterix indicates that $m_H$ is evaluated for $T_X$ at the LEP II upper limit from table 4.

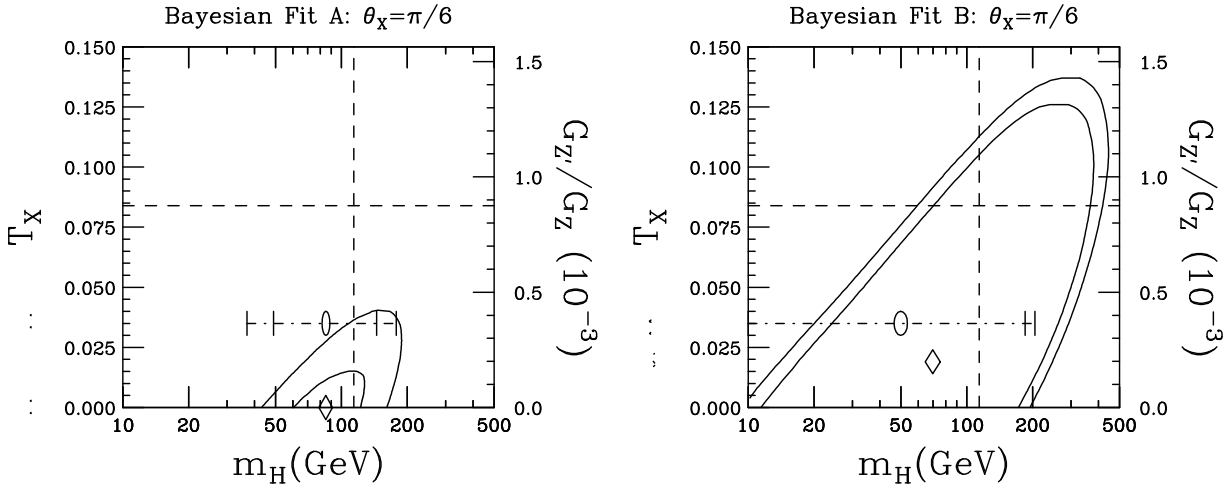


Figure 9: 90% and 95% CL Bayesian contours for $Z'$ model with $\theta_X = \pi/6$, as in figure 8.

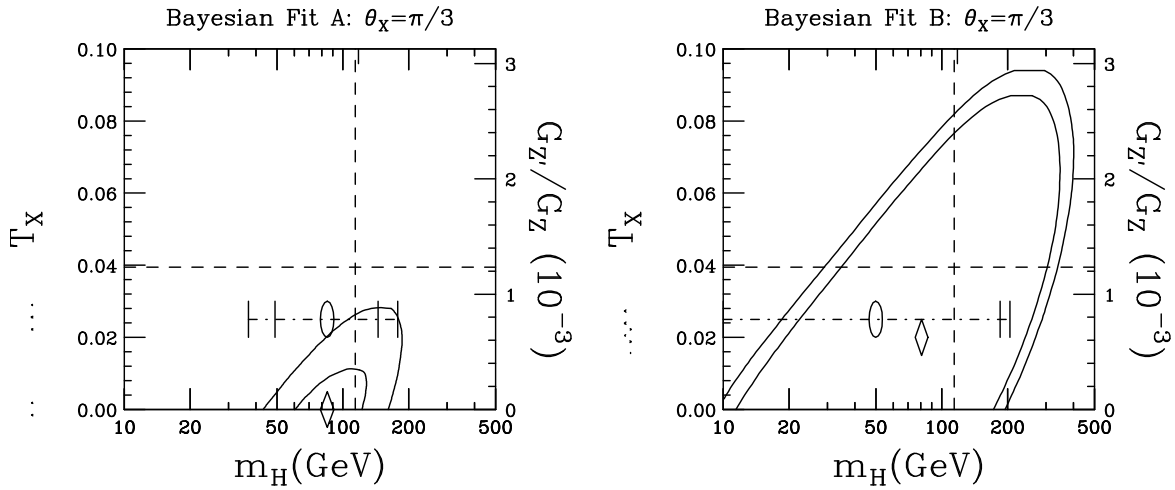


Figure 10: 90% and 95% CL Bayesian contours for $Z'$ model with $\theta_X = \pi/3$, as in figure 8.

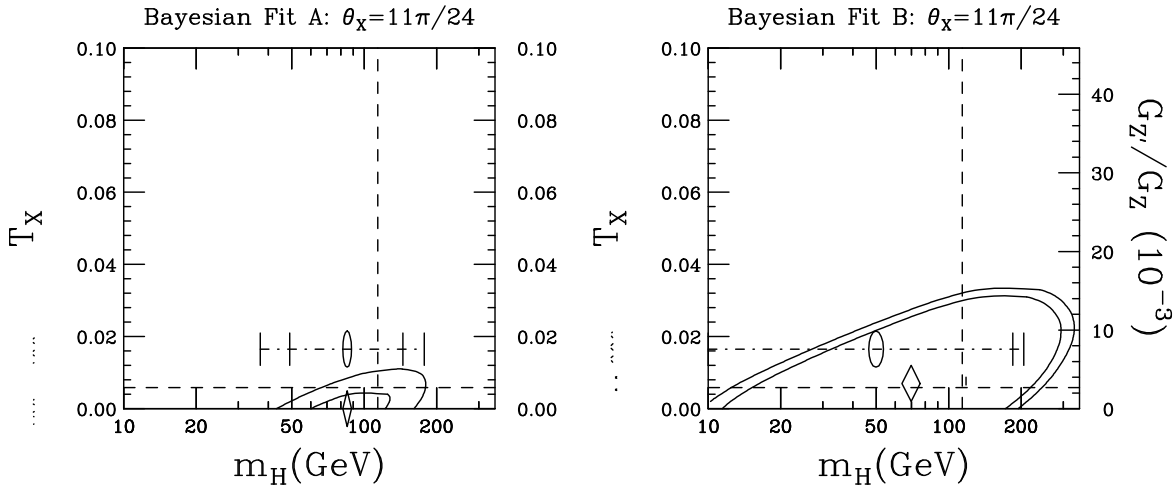


Figure 11: 90% and 95% CL Bayesian contours for $Z'$ model with $\theta_X = 11\pi/24$, as in figure 8.

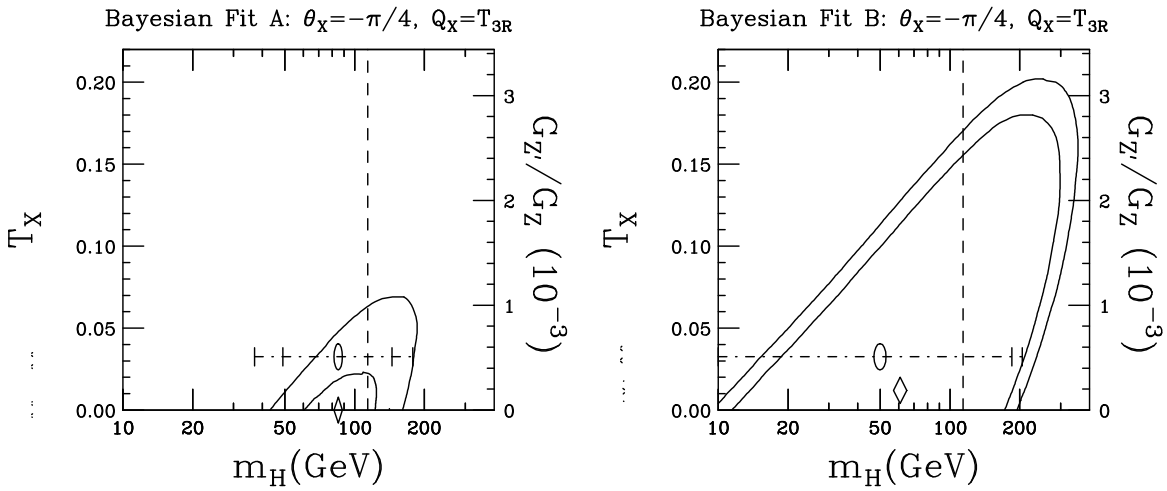


Figure 12: 90% and 95% CL Bayesian contours for $Z'$ model with $\theta_X = -\pi/4$, $Q_X = T_{3R}$, as in figure 8. The LEP II upper limit, $T_X < 0.30$, is off the graph.

fit, and since they have one fewer degree of freedom the CL is lower than the SM, reaching 0.10 at a smaller value of $m_H$. The opposite is true of the Bayesian fits to set B, for which the $\chi^2$ minima in the $Z'$ models are appreciably lower than in the SM, occuring at larger $T_X$ , and the robust CL allows for larger values of $m_H$ before the $\chi^2$ probability falls to 0.10. In the frequentist fits of $Z'$ models using the $\Delta\chi^2$ method, $m_H$ also reaches larger values for set B than for set A, but in that case the effect is due entirely to the improvements in the fit at larger $m_H$ from $Z - Z'$ mixing and not at all to the more robust SM fit of set B.

The effect of the CDF bounds on the predictions of the Bayesian fits for the Higgs boson mass is shown in table 12. There is little effect on the fits to data set A since the bounds on $T_X$ from the EW fits alone are already very strong. In the case of data set B the CDF bounds have more impact, especially for smaller $g_{Z'}$.

## 6. Discussion

We have explored the effect of a conservative class of $Z'$ models on the Higgs mass prediction from the EW fits, considering both the possiblity that the discrepancy is a statistical fluctuation and that it is the result of underestimated systematic uncertainty. In the first case we fitted essentially all the precision EW data, data set A, while in the second we considered the data without the three hadronic asymmetry measurements, data set B. The fits show that the range of allowed values for $m_H$ can be significantly expanded into the allowed region above 114 GeV for data set B while retaining an acceptable fit to the precision data, but for data set A the possiblities are more restricted. In particular, because of the marginal confidence level of the SM fit to data set A, the Bayesian fits of the $Z'$ models allow even smaller domains for $m_H$ than the SM.

| Model | r | Data Set A | | Data Set B | |
|---|---|---|---|---|---|
| | | $m_H(95\%)$ CDF | $m_H(95\%)$ LEP II | $m_H(95\%)$ CDF | $m_H(95\%)$ LEP II |
| | 0.27 | 127 | | 384 | |
| $\theta_X = 0$ | 0.13 | 127 | 127 | 254 | 390 |
| | 0.081 | 127 | | 211 | |
| | 0.20 | 128 | | 302 | |
| $\pi/6$ | 0.098 | 128 | 128 | 220 | 368 |
| | 0.059 | 123 | | 195 | |
| | 0.20 | 128 | | 235 | |
| $\pi/3$ | 0.098 | 128 | 128 | 196 | 300 |
| | 0.059 | 128 | | 188 | |
| | 0.24 | 128 | | 190 | |
| $11\pi/24$ | 0.12 | 125 | 128 | 180 | 220 |
| | 0.072 | 124 | | 176 | |

Table 12: Effect of CDF bounds on the Higgs boson mass from Bayesian fits of data sets A and B. As in table 11, $m_H(95\%)$ is the maximum value of $m_H$ on the 90% Bayesian contours (figures 8 - 12) that is consistent with the CDF direct limit on $T_X$ for given values of $r = g_Z/g_{Z'}$. The values of $m_H(95\%)$ required by the LEP II bounds on $T_X$, which are independent of $r$, are shown for comparison.

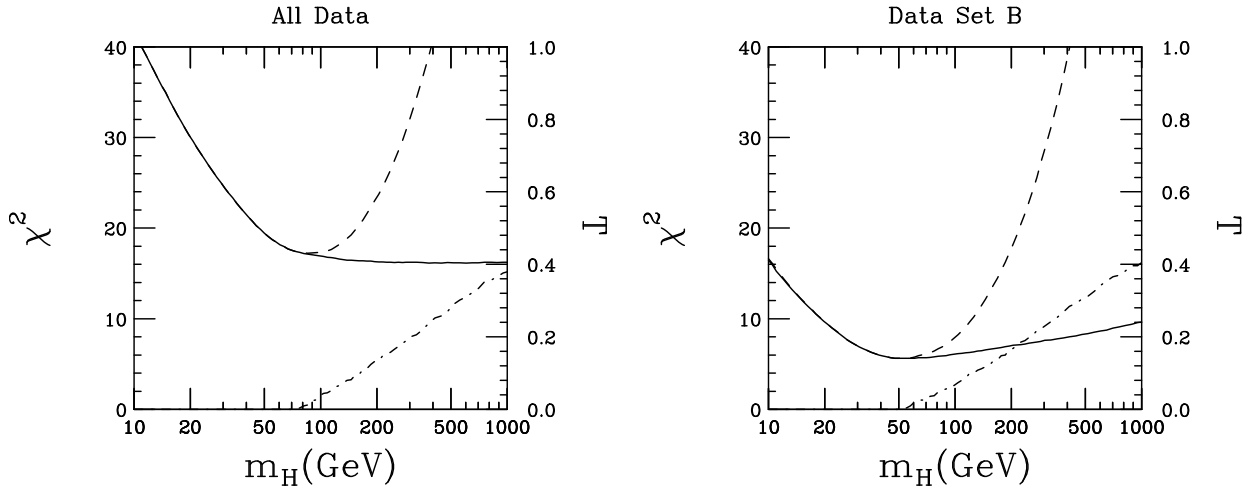


Figure 13: $\chi^2$ fits to the complete data set of Table 1 and to data set B with the oblique parameter $T > 0$. The solid line is the $\chi^2$ distribution for the oblique fit, with the corresponding value of $T$ shown in the dot-dashed line which is read to the right axis. The dashed line is the $\chi^2$ distribution for the SM fit.

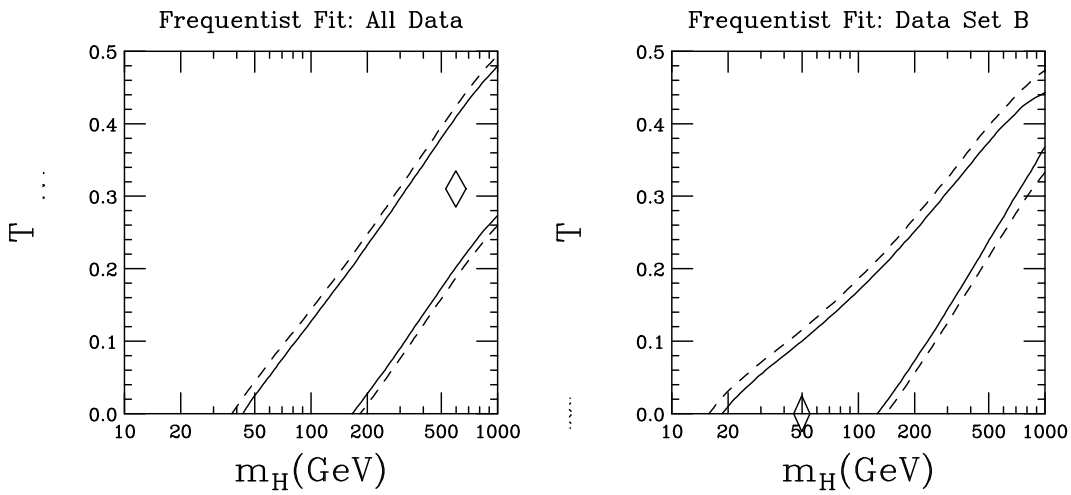


Figure 14: 90 (solid line) and 95% (dashed line) contour plots of frequentist fits with oblique parameter $T > 0$. The position of the $\chi^2$ minimum is indicated by the diamond.

This is likely to be a generic feature of the response of the two data sets to models of new physics, because it is typically easier to construct models that raise the prediction for $m_H$ than it is to address the peculiarities of the $A^b_{FB}$ anomaly, as would be necessary to raise the marginal confidence level of the fit to data set A. For instance, obliquely mediated weak isospin breaking can raise the prediction for $m_H$ toward the TeV scale without impairing the quality of the fits but cannot improve them significantly. Figure 13 shows that fits with the oblique parameter $T > 0$, which generically represents weak isospin breaking mediated by vacuum polarization, can flatten the $\chi^2$ distribution for large values of $m_H$, for both the fit to the complete data set with 12 $dof$ and for the fit to data set B with 9 $dof$. The $\chi^2$ confidence levels of these fits, $\simeq 0.13$ for the complete set and $\simeq 0.7$ for set B, are very near the CL's of the corresponding SM fits at their $\chi^2$ minima.

Figures 14 and 15 display the 90 and 95% confidence level contour plots in the $m_H, T$ plane for frequentist and Bayesian fits. In a reversal of what we found for the $Z'$ models, the $\chi^2$ minimum for the all-data set is at nonzero $T$ with elevated $m_H$, while for fit B it coincides with the SM fit with $T = 0$ and $m_H = 50$ GeV. However the position of the $\chi^2$ minima are not very significant, since the minima are extremely shallow, as is evident in figure 13.

Weak isospin breaking is the basis for the effect of $Z - Z'$ mixing on the $m_H$ predictions presented here. In the $Z'$ models the effect is limited to $m_H \lesssim 300$ GeV because the shifts in the $Z\overline{f}f$ couplings are proportional to $g_{Z'}\theta_M$, which in turn is proportional to $T_X$,

$$g_{Z'}\ \theta_M = g_Z \frac{\alpha T_X}{\cos\theta_X}. \tag{28}$$

The limit on $T_X$ is reached when $g_{Z'}\ \theta_M$ grows so large that the $Z\overline{f}f$ couplings deviate too far from their SM values, causing $\chi^2$ to increase.

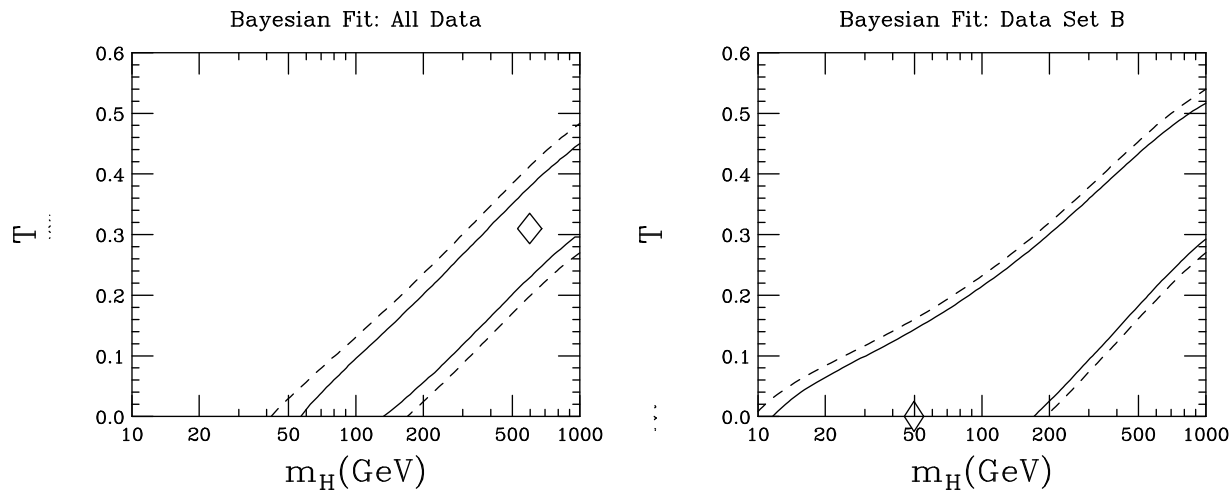


Figure 15: 90 (solid line) and 95% (dashed line) contour plots of Bayesian fits with oblique parameter $T > 0$. The position of the $\chi^2$ minimum is indicated by the diamond.

The $3.2\sigma$ discrepancy in the SM determination of the weak mixing angle by leptonic and hadronic asymmetry measurements sends an ambiguous message. It reduces the confidence level of the SM fit and raises questions about the SM prediction for $m_H$, which averages a "bimodal" distribution of measurements favoring 50 ($A_{LR}$, $m_W$) and 500 GeV ($A^b_{FB}$), as shown in figure 1. The significance and meaning of the discrepancy can only be clarified by future experimental data. If for instance evidence is found for a large deviation of the right-handed $Z\bar{b}b$ coupling from its SM value, it would confirm the $A^b_{FB}$ anomaly as a genuine signal of new physics. If the discrepancy results from unresolved theoretical and/or experimental systematic uncertainties in the very challenging hadronic asymmetry measurements, the low SM prediction for $m_H$ that results from the remaining measurements (data set B) strongly suggests new physics to raise the predicted value into the experimentally allowed region.

The simple class of models studied here offers a paradigm for how we can use the LHC together with the precision EW data to understand the underlying physics. If a $Z'$ boson is discovered at the LHC, it will be important to compare its properties as measured at the LHC with the constraints of the EW fits. It would first be essential to study the leptonic and hadronic couplings of the $Z'$ to determine whether it is in fact in the class of $Z'$ bosons considered here and to measure the parameter $\theta_X$. If so, the measurement of the coupling constant $g_{Z'}$ and mass $m_{Z'}$ would determine the effective Fermi constant $G_{Z'}$, which in turn specifies the oblique parameter $T_X$ that determines the $Z'$ fits. With the $Z'$ parameters known, the EW fit would make a prediction for the Higgs boson mass which could be compared with direct measurement of $m_H$ at the LHC. It is then important to ascertain how well such a program could be carried out at the LHC,[19] both in its original incarnation and after possible luminosity and energy upgrades.

This example illustrates the important role that the precision EW data can continue to play in the future. At the end of the day, when new physics has been discovered and studied at the LHC, we will want to consider how it affects the EW fit. A consistent explanation of both the high energy data and the precision EW data would be a powerful confirmation of the theoretical picture, just as high energy data together with the precision data have confirmed the SM as the correct zero'th order model. If the model used to describe the high energy measurements is not consistent with the precision EW data, it could mean that the model is wrong or that there is other undiscovered new physics affecting the EW observables.

To realize the potential of such a program, combining both the high energy measurements and the low energy precision data, it is important to resolve the ambiguity that the $A^b_{FB}$ anomaly casts over the current data. Future high statistics studies at a high intensity Z factory like the proposed Giga-Z project[20] could determine if the anomaly is a statistical fluctuation and would allow further study of the experimental systematic uncertainties. Additional work on systematic uncertainties with a theoretical component would also be essential, for instance, the merging of the radiative corrections to $Z \to \bar{b}b$ with the experimental acceptance, which gives rise to a systematic uncertainty that is now very difficult to quantify.

It is also possible that the LHC could illuminate the issue. For instance, in the framework of the models discussed in this paper, the discovery of a $Y$-sequential $Z'$ boson together with a 300 GeV Higgs boson would be compatible with the Bayesian fit to data set B but not to data set A. In general, discoveries at the LHC could favor a model that is consistent with one data set but not the other. The EW fit of the compatible data set could then be compared with the direct observations at the LHC to further constrain and test the model. In principle, if the ambiguities can be resolved and the precision can be improved, the EW fit could even be used to probe for additional new physics before it is directly observed, just as the radiative corrections to the rho parameter[21] enabled the prediction of the top quark mass scale before the top quark was discovered.

## Appendix: "Pseudo-Oblique" Parameterization of the $Y$-Sequential Model

We will show, as discussed in section 3, that the effect of mixing with $Y$-Sequential $Z'$ bosons on the EW fits discussed here can be represented by oblique parameters $S', T'$, given by

$$T' = -T_X \tag{A1}$$

$$S' = -4(1 - x_W)T_X \tag{A2}$$

where from equation (17) with $\theta_X = 0$

$$\alpha T_X = \epsilon = -\frac{\delta m_Z^2}{m_Z^2}. \tag{A3}$$

The precision EW fit for the $Y$-sequential $Z'$ boson model can then be extracted from the usual oblique fit by considering the line $S = 4(1 - x_W)T$ in the $S, T$ plane.

Using equations (12 - 16) with $\theta_X = 0$, the $Z\overline{f}f$ interaction, equation (11), is

$$\mathcal{L}_f = g_Z \left(1 + \frac{\alpha T_X}{2}\right) \overline{f} \not{Z} (t_{3L}^f - q^f \hat{x}_W + \epsilon \frac{y}{2}) f. \tag{A4}$$

We will show that the interaction can also be represented by the obliquely corrected SM Lagrangian

$$\mathcal{L}_f = g_Z \left(1 + \frac{\alpha T'}{2}\right) \overline{f} \not{Z} (t_{3L}^f - q^f x'_W) f. \tag{A5}$$

where $x'_W$ has the usual oblique correction in terms of $S'$ and $T'$,

$$x'_W - x_W = \frac{\alpha}{1 - 2x_W} \left(\frac{S'}{4} - x_W(1 - x_W)T'\right) \tag{A6}$$

and the $W$ boson mass also gets the ususal correction,

$$\frac{\delta m_W^2}{m_W^2} = \frac{\alpha}{1 - 2x_W} \left(-\frac{S'}{2} + (1 - x_W)T'\right). \tag{A7}$$

To obtain equations (A5) and (A6) we substitute $y = 2(q - t_3)$ in equation (A4). The result to order O($\epsilon$) is

$$\mathcal{L}_f = g_Z \left(1 + \frac{\alpha T_X}{2} - \epsilon\right) \overline{f} \not{Z} [t_{3L}^f - q^f (\hat{x}_W - \epsilon(1 - x_W))] f. \tag{A8}$$

Matching the prefactors of equations (A5) and (A8) implies that $\alpha T' = \alpha T_X - 2\epsilon = -\alpha T_X$, which establishes equation (A1). $S'$ is then fixed by the remaining condition for the equivalence of equations (A5) and (A8), $x'_W = \hat{x}_W - \epsilon(1 - x_W)$, which implies

$$\frac{\alpha}{1 - 2x_W} \left(\frac{S'}{4} - x_W(1 - x_W)T'\right) = -\alpha T_X \left(\frac{x_W(1 - x_W)}{1 - 2x_W} + 1 - x_W\right) \tag{A9}$$

and using equation (A1) yields the result, equation (A2), for $S'$.

The corrections to the $W$ boson mass now provide a nontrivial test of the equivalence of the $S'$, $T'$ oblique representation with the original $Z'$ model. From the original model the correction is

$$\frac{\delta m_W^2}{m_W^2} = \frac{1 - x_w}{1 - 2x_w} \alpha T_X. \tag{A10}$$

Substituting the expressions for $S'$ and $T'$ in terms of $T_X$ from equations (A1) and (A2) into the generic expression for $\delta m_W$, equation (A7), the result is precisely equation (A10). For all other observables we consider (see table 1) the oblique corrections enter via the weak mixing angle $x_W$ or, in the case of the $Z$ width $\Gamma_Z$, via the prefactor $1 + \alpha T$. We are then

guaranteed that oblique fits with the constraint $S' = 4(1 - x_w)T'$ are equivalent to the fits of the original $Y$-sequential $Z'$ model. We have also verified the equivalence numerically by fitting the data using both representations.

This work was supported in part by the Director, Office of Science, Office of High Energy and Nuclear Physics, Division of High Energy Physics, of the U.S. Department of Energy under Contract DE-AC02-05CH11231

# References

[1] The ALEPH, DELPHI, L3, OPAL, SLD Collaborations, the LEP Electroweak Working Group, the SLD Electroweak and Heavy Flavour Groups, Physics Reports: Volume 427 Nos. 5-6 (May 2006) 257-454, hep-ex/0509008.

[2] M. Chanowitz, Phys.Rev.Lett.87:231802,2001, hep-ph/0104024; M. Chanowitz, Phys.Rev.D66:073002,2002, hep-ph/0207123; M. Chanowitz, Presented at Mini-Workshop on Electroweak Precision Data and the Higgs Mass, Zeuthen, Germany, 28 Feb - 1 Mar 2003. Published in *Zeuthen 2003, Electroweak precision data and the Higgs mass* 15-24 e-Print: hep-ph/0304199. See also the talk posted at http://theory.fnal.gov/jetp/talks/chanowitz.pdf.

[3] Guido Altarelli *et al.*, JHEP 0106:018,2001.

[4] V.A. Novikov, L.B. Okun, Alexandre N. Rozanov, Phys.Lett.B529:111-116,2002, e-Print: hep-ph/0111028; JETP Lett.76:127-130,2002, Pisma Zh.Eksp.Teor.Fiz.76:158-161,2002, e-Print: hep-ph/0203132.

[5] F. del Aguila, J. de Blas, M. Perez-Victoria, UG-FT-224-08, CAFPE-94-08, Mar 2008. 31pp. e-Print: arXiv:0803.4008 [hep-ph]

[6] A. Ferroglia, A. Lorca, J.J. van der Bij, Annalen Phys.16:563-578,2007, e-Print: hep-ph/0611174.

[7] A.B. Arbuzov *et al.*, Comput.Phys.Commun.174:728-758,2006. e-Print: hep-ph/0507146.

[8] Marcela S. Carena, Alejandro Daleo, Bogdan A. Dobrescu, Tim M.P. Tait. FERMILAB-PUB-04-129-T, Aug 2004. 34pp. Published in Phys.Rev.D70:093009,2004. e-Print: hep-ph/0408098

[9] LEP Collaboration, hep-ex/0312023

[10] CDF Collaboration (A. Abulencia et al.). Phys.Rev.Lett.**96**:211801,2006. e-Print: hep-ex/0602045

[11] Michael S. Chanowitz, John R. Ellis, Mary K. Gaillard. CERN-TH-2312, May 1977, 45pp. Published in Nucl.Phys.B128:506,1977.

[12] Thomas Appelquist, Bogdan A. Dobrescu, Adam R. Hopper. YCTP-11-02, FERMILAB-PUB-02-307-T, Dec 2002. 25pp. Published in Phys.Rev.D68:035012,2003. e-Print: hep-ph/0212073

[13] M. Awramik, M. Czakon, A. Freitas, G. Weiglein. DCPT-03-146, DESY-03-184, FERMILAB-PUB-03-239-T, IPPP-03-73, Nov 2003. 10pp. Published in Phys.Rev.D69:053006,2004. e-Print: hep-ph/0311148; M. Awramik, M. Czakon, A. Freitas. DESY-06-108, ZH-TH-17-06, Aug 2006. 28pp. Published in JHEP 0611:048,2006. e-Print: hep-ph/0608099.

[14] Tevatron Electroweak Working Group for the CDF and D0 Collaborations, March, 2008, arXiv:0803.1683 [hep-ex].

[15] The most recent EWWG fit is posted at http://lepewwg.web.cern.ch/LEPEWWG/plots/winter2008/.

[16] See for instance D. Choudhury, T.M.P. Tait, C.E.M. Wagner, Phys.Rev.D65:053002,2002; Xiao-Gang He and G. Valencia, Phys.Rev.D68:033011,2003, e-Print: hep-ph/0304215; D.E. Morrissey and C.E.M. Wagner, Phys.Rev.D69:053001,2004, e-Print: hep-ph/0308001; Rodolfo A. Diaz, R. Martinez, F. Ochoa, Phys.Rev.D72:035018,2005, e-Print: hep-ph/0411263; Abdelhak Djouadi, Gregory Moreau, Francois Richard, Nucl.Phys.B773:43-64,2007, e-Print: hep-ph/0610173.

[17] B. Holdom, Phys. Lett. B 259:329, 1991.

[18] Michael Edward Peskin, Tatsu Takeuchi, Phys.Rev.D46:381-409,1992.

[19] See for instance G. Bozzi, B. Fuks, and M. Klasen, Nucl.Phys.**B794**:46,2008; B. Fuks *et al.*, Nucl.Phys.**B797**:322,2008.

[20] ECFA/DESY LC Physics Working Group, J.A. Aguilar-Saavedra *et al.*, hep-ph/0106315 and references therein.

[21] M. Veltman, Acta Phys.Polon.B8:475,1977; M. Chanowitz, M. Furman, I. Hinchliffe, Phys.Lett.B78:285,1978 and Nucl.Phys.B153:402,1979.